J Mol Model (2012) 18:4965–4984
DOI 10.1007/s00894-012-1492-2

ORIGINAL PAPER

Structure and functional features of olive pollen pectin methylesterase using homology modeling and molecular docking methods

Jose C. Jimenez-Lopez · Simeon O. Kotchoni · María I. Rodríguez-García · Juan D. Alché

Received: 19 April 2012 / Accepted: 4 June 2012 / Published online: 22 June 2012

Abstract Pectin methylesterases (PMEs), a multigene family of proteins with multiple differentially regulated isoforms, are key enzymes implicated in the carbohydrates (pectin) metabolism of cell walls. Olive pollen PME has been identified as a new allergen (Ole e 11) of potential relevance in allergy amelioration, since it exhibits high prevalence among atopic patients. In this work, the structural and functional characterization of two olive pollen PME isoforms and their comparison with other PME plants was performed by using different approaches: (1) the physicochemical properties and functional-regulatory motifs characterization, (2) primary sequence analysis, 2D and 3D comparative structural features study, (3) conservation and evolutionary analysis, (4) catalytic activity and regulation based on molecular docking analysis of a homologue PME inhibitor, and (5) B-cell epitopes prediction by sequence and structural based methods and protein-protein interaction tools, while T-cell epitopes by inhibitory concentration and binding score methods. Our results indicate that the structural differences and low conservation of residues, together with differences in physicochemical and posttranslational motifs might be a mechanism for PME isovariants generation, regulation, and differential surface epitopes generation. Olive PMEs perform a processive catalytic mechanism, and a differential molecular interaction with specific PME inhibitor, opening new possibilities for PME activity regulation. Despite the common function of PMEs, differential features found in this study will lead to a better understanding of the structural and functional characterization of plant PMEs and help to improve the component-resolving diagnosis and immunotherapy of olive pollen allergy by epitopes identification.

Keywords Allergen · Cell wall · Homology modeling · Molecular docking · *Olea europaea* L. · Pectin · Pollen

Electronic supplementary material The online version of this article (doi:10.1007/s00894-012-1492-2) contains supplementary material, which is available to authorized users.

J. C. Jimenez-Lopez
Department of Biological Sciences, College of Sciences,
Purdue University,
201 S. University Street,
West Lafayette, IN 47906, USA

S. O. Kotchoni
Department of Biology, Rutgers University,
315 Penn St.,
Camden, NJ 08102, USA

S. O. Kotchoni
Center for Computational and Integrative Biology (CCIB),
Rutgers University,
315 Penn St.,
Camden, NJ 08102, USA

J. C. Jimenez-Lopez (✉) · M. I. Rodríguez-García · J. D. Alché
Department of Biochemistry, Cell and Molecular Biology of Plants, Estación Experimental del Zaidín, High Council for Scientific Research (CSIC),
Profesor Albareda 1,
Granada 18008, Spain
e-mail: jcjimenezl75@gmail.com

Introduction

Pectin methylesterases (PMEs) catalyze the removal of carboxymethyl ester groups of the homo/polygalacturonate (H/PG) chain from pectins, one of the main components of plant cell wall, giving rise to domains of contiguous deesterified galacturonic acid residues [1]. PME activities are regulated by endogenous pectin methylesterase inhibitors (PMEIs) that control the degree of methylesterification of

homogalacturonate (HG) [2]. Thus, the regulation of interaction between PME and PMEI, and the inhibitory mechanism are of significant interest, not only in plant physiological processes but also in food technology.

PMEs have been found in pathogenic bacteria, yeast [3, 4], insect [5], and higher plants (peach, tomato, potato, kiwi, carrot, flax or strawberry) [6], where they have been implicated in the remodeling of the plant cell wall during ripening, and growth in differentially expressed vegetative tissues [7]. To date, only the crystal three-dimensional structure of three bacterial PMEs: *Erwinia chysanthemi*, *Yersinia enterocolitica*, and *Dickeya dadantii*, and two plant PMEs, *Daucus carota* and *Solanum lycopersicum* have been elucidated (www.pdb.org). The expression analysis of plant pectin-degrading enzymes at different developmental stages, and the high number of isoforms existent, i.e., 69 in *Arabidopsis* (TAIR, www.arabidopsis.org), suggesting that these enzymes play important roles in a wide range of physiological processes such as development and plant growth, morphogenesis, organogenesis, leaf abscission, root development [8], stem cell differentiation and fiber length determination in trees [9], seed hydration and germination, fruit maturation and dehiscence [10]. In pollen, PMEs are involved in reproduction processes such as microsporogenesis and male fertility. They also play a central role in the reorganization of the pollen wall during germination and pollen tube growth, as well as in the control of cell elongation during the pollen tube growth [11]. In addition, PMEs have also been reported to act in the defense mechanisms of plants against pathogens [12, 13].

Furthermore, PMEs have been typically recognized as IgE-inducers of allergy symptoms. Olive (*Olea europaea* L.) pollen is one of the main causes of respiratory type-I allergy, an increasing clinical disorder that is mediated by the production of IgE antibodies. It affects more than 25 % of the human population around the world [14], especially in Mediterranean areas, as well as some areas in America, and Australia. To date, 12 allergens (Ole e 1–12) have been identified in olive pollen [15]. The functional assessment of the last two allergens identified in pollen, Ole e 11 as PME [16], and Ole e 12 as a phenylcoumaran benzylic ether reductase (Genebank accession number ACL13551) has been characterized based on gene and/or protein sequence similarity to other plant species.

In this study we performed a comprehensive molecular, structural and functional analysis of olive PMEs based on built protein homology models of two isoforms of Ole e 11 currently available in public databases, in addition, to their counterparts in others plant species. We also identified and structurally characterized the B- and T-cell epitopes of olive PMEs by following different *in silico* approaches. This paper reflects the importance of assessing the 3D molecular structure and allergenic features of PMEs by focusing on different strategies to efficiently tackle allergy symptoms throughout diagnosis and therapy developments, while emphasizing structural function and regulatory relationship characterization of PMEs and their impacts in plant-derived food industry.

Materials and methods

PMEs sequences database search

Olive PME (Ole e 11 allergen) sequence isoforms, Ole e 11.0101 (NCBI accession number ACZ57582) and Ole e 11.0102 (NCBI accession number AAY88919) were used as queries to search for pollen and vegetative PMEs against publicly available sequence databases Swiss-Prot/TrEMBL (Uniprot) (www.uniprot.org), and NCBI (www.ncbi.nlm.nih.gov) using BLASTX, BLASTN and BLAST (low complexity filter, Blosum62 substitution matrix) (blast.ncbi.nlm.nih.gov/Blast.cgi).

Domain architecture analyses

In order to investigate the possible domains in Ole e 11 protein isoforms, we performed additional domain specific database queries. In this regard, Characteristic motifs and patterns were additionally queried using Pfam v25.0 (pfam.sanger.ac.uk), Prosite (prosite.expasy.org/scanprosite), SMART v6.0 (smart.embl-heidelberg.de), Conserved Domain Database (CDD) v3.02, CDART (Conserved Domain Architecture Retrieval Tool) and CD-Search tools (www.ncbi.nlm.nih.gov/Structure/cdd/cdd.shtml), InterPRO v35.0 (www.ebi.ac.uk/interpro), ProDom release 2010.1 (prodom.prabi.fr/prodom/current/html/home.php), CATH v3.4 (www.cathdb.info), Superfamily v1.75 (supfam.cs.bris.ac.uk/SUPERFAMILY), PIRSF (pir.georgetown.edu), and functional search by PANTHER (www.pantherdb.org).

Phylogenetic analysis of pollen PMEs

Amino acid sequences of the 23 retrieved pollen PMEs were used to make alignments using ClustalW multiple sequence alignment tool (www.ebi.ac.uk/Tools/clustalw). The alignments data were used for homology modeling of Ole e 11 isoform proteins. These alignments were created using the Gonnet protein weight matrix, multiple alignment gap opening/extension penalties of 10/0.5 and pairwise gap opening/extension penalties of 10/0.1. The outputs were manually checked to optimize the alignment by using Bioedit (www.mbio.ncsu.edu/bioedit/bioedit.html). Phylogenetic trees were generated by the neighbor-joining method (NJ), and the branches were tested with 1000 bootstrap replicates. Trees were visualized using Treedyn (www.treedyn.org).

Physicochemical properties and post-translational patterns/motifs

The physicochemical properties of the profilin sequences were analyzed using the Expert Protein Analysis System (ExPASy) Proteomics Server (expasy.org). The ProtParam tool was implemented to calculate the MW/pI of the different PME isoforms, as well as the instability index, aliphatic index and grand average of hydropathicity (GRAVY).

PME characteristic patterns were checked for each original sequence and further analyses were performed to highlight the presence of functional motifs using the PROSITE database (prosite.expasy.org). Biologically meaningful motifs and susceptibility to posttranslational modifications were derived from multiple alignments and the ScanProsite tool (prosite.expasy.org), from the ExPASy proteomics server of the Swiss Institute of Bioinformatics. Phosphorylation motifs with more than 80 % of probability of occurrence were analyzed by using NETPhos v2.0 and NETPhosK v1.0 (www.cbs.dtu.dk).

Secondary structure prediction

Recognition of Ole e 11 secondary structural elements was assessed by Segmer algorithm [17], which threads sequence segments through the Protein Data Bank (PDB) library (www.pdb.org) to identify conserved substructures. Furthermore, elements of the secondary structure were also identified, and compared with the results obtained with other different approaches: SSpro8 (Scratch Protein Predictor), which adopts the full DSSP 8-class output classification (scratch.proteomics.ics.uci.edu), PredictProtein (www.predictprotein.org), NetSurfP ver. 1.1 (www.cbs.dtu.dk), and PSIPRED (bioinf.cs.ucl.ac.uk/psipred) fold servers.

Structure templates searching

The sequences of the two Ole e 11 isoforms were searched for homology in the Protein Data Bank (PDB). Homologous templates suitable for Ole e 11, as well as for others plant species were selected by BLAST server (ncbi.nlm.nih.gov). The BioInfoBank Metaserver (meta.bioinfo.pl), which employs fold recognition for homology search, was also used for the selection of templates. Furthermore, the results obtained by previous methods were also compared with the results obtained by Swiss-model server for template identification (swissmodel.expasy.org). Five best templates (1GQ8, 1XG2, 1QJV, 2NTP, 2NSP) were used for homology modeling.

Homology modeling

Homology modeling was performed by SWISS-MODEL, via the ExPASy web server (swissmodel.expasy.org). An initial structural model was generated for the different PMEs members and checked for recognition of errors in 3D structures using ProSA (prosa.services.came.sbg.ac.at/prosa.php), and for a first overall quality estimation of the model with QMEAN (swissmodel.expasy.org/qmean/cgi/index.cgi).

Final structures were subjected to energy minimization with GROMOS96 force field energy implemented in DeepView/Swiss-PDBViewer v3.7 (spdbv.vital-it.ch) to improve the van der Waals contacts and correct the stereochemistry of the model. For each sequence analyzed, the quality of the model was assessed by QMEAN, checking proteins stereology with PROCHECK (www.ebi.ac.uk/thornton-srv/software/PROCHECK), ProSA, and Errat (nihserver.mbi.ucla.edu/ERRATv2) programs, as well as the protein energy with ANOLEA (protein.bio.puc.cl/cardex/servers/anolea). The Ramachandran plot statistics for the models were also calculated to show the number of protein residues in the favored regions.

Ligand-binding domains and functional annotation based on 3D protein structures

Prediction of the best identified ligand-binding sites or domains in the PME built structures were made through primary sequence and structure-based approaches to protein functional inference and ligand screening. This approach uses a threading algorithm based on binding site conservation across evolutionary distant proteins for ligand binding site prediction, ligand screening and molecular functional prediction.

Cofactor software (zhanglab.ccmb.med.umich.edu/COFACTOR), a structure-based method for biological function annotation of proteins was used in providing a 3D-structural model of the protein of interest to identify functional homology. Functional insights, including ligand-binding site, and enzyme classification, were derived from the best functional homology template. The identification of functional analogs of the query proteins were possible by Gene Ontology (GO) terms (The Gene Ontology project), based on built 3D models, describing the molecular function and biological processes in which proteins are implicated (www.geneontology.org).

Structural comparison and evolutionary conservation analysis

Structural comparisons between Ole e 11 isoforms and other plant PMEs were performed by superimposition of the structural Cα carbons, aiming to calculate the average distance between their Cα backbones. The 2-D protein structural analysis, protein superimpositions and surface protein contours analysis were performed and visualized in PyMol software (www.pymol.org). Built protein models were submitted to ConSurf server (consurf.tau.ac.il) in order to

generate evolutionary related conservation scores, helping us to identify functional region in the proteins. Functional and structural key residues in the PME sequences were confirmed by ConSeq server (conseq.tau.ac.il).

Poisson–Boltzmann electrostatic potential

The electrostatic Poisson-Boltzmann (PB) potentials for the structures were obtained using APBS molecular modeling software implemented in PyMol 0.99 (www.pymol.org) with AMBER99 to assign the charges and radii to all the atoms (including hydrogens), and optimized with the Python software package PDB2PQR. Fine grid spaces of 0.35 Å were used to solve the linearized PB equation in sequential focusing multigrid calculations in a mesh of 130 points per dimension at 310.00 K. The dielectric constants were two for the proteins and 80.00 for water. The output mesh was processed in the scalar OpenDX format to render the isocontours and maps on the surfaces with PyMOL 0.99. Potential values are given in units of kT per unit charge (k Boltzmann's constant; T temperature).

Protein docking process and clustering analysis

In order to get functional insights and to evaluate the interaction between PME and its inhibitors, we performed the docking analysis between Ole e 11 proteins and PME inhibitors from the closer-structural species, *Daucus carota* (Uniprot accession number P17407). We considered the backbone flexibility by using rigid-body ensemble docking with multiple structures derived from NMR. The Fast Fourier Transform (FFT) correlation approach to protein-protein docking evaluates the energies of billions of docked conformations on a grid. To obtain decoys by rigid-body docking, we used the option ZDOCK for sampling at 6-degree rotational steps in CLUSpro [18]. Using Fast Fourier Transform, ZDOCK searches for all possible binding orientations of a ligand along the surface of a receptor protein, optimizing desolvation, shape complementarily, and electrostatics. The top 2000 structures, along with their ZDOCK scores, were used as candidates of near-native structures. The docking score was calculated by considering several interaction properties, e.g., shape complementarity, desolvation, and electrostatics potential.

Since we cluster binding site RMSDs, for each docked conformation, we need to compute the residues of the ligand within 10 Å of its receptor, and the RMSD of these residues with all 2000 ligands. After clustering, the ranked complexes are subjected to a straightforward (300 step and fixed backbone) van der Waals minimization using CHARMM to remove potential side chain clashes. Best scoring protein-inhibitor structure was chosen as higher possible model for PME-protein inhibitor interaction.

Allergenicity profile assessment

Allergenicity of both isoforms was checked by a full FASTA alignment in the Structural Database of Allergenic Proteins (SDAP) (fermi.utmb.edu/SDAP). Allergenicity profile was assessed by combination of different parameters: hydrofobicity, and antigenicity. Solvent accessible surface areas (SASA) of all residues in the generated models were calculated by using GETAREA (curie.utmb.edu/getarea.html), and compared to absolute surface area (ASA) of each residue calculated by DSSP program (swift.cmbi.ru.nl/gv/dssp). These values were transformed to relative values of ASA and visualized by ASAView (www.netasa.org/asaview).

B-cell epitopes identification

For determination of linear (continues) epitopes, the sequence of Ole e 11 isoform proteins were submitted to ABCpred (www.imtech.res.in/raghava), BepiPred (www.cbs.dtu.dk), BCPREDS (ailab.cs.iastate.edu/bcpreds), Bcepred (www.imtech.res.in/raghava), Ellipro (tools.immuneepitope.org), and COBEpro (scratch.proteomics.ics.uci.edu) web servers.

For prediction of discontinuous (conformational) epitopes, the best structures generated by homology modeling were submitted to Discotope 1.2 server (www.cbs.dtu.dk), BEpro (pepito.proteomics.ics.uci.edu/index.html), and PPI-PRED (bmbpcu36.leeds.ac.uk/ppi_pred). The methods were selected on the basis of performance measures that include both threshold dependent (sensitivity, specificity, accuracy) and independent parameters. While selecting consensus epitopes, a preference was given to results predicted from tools tested on larger datasets and having an area under receiver operating characteristic curve (AUC) greater than 0.70. Tools based solely on physicochemical parameters were given lower preference. Default settings were applied to all the tools used. The regions recognized frequently by at least four tools were selected.

T-cell epitopes identification

Stabilization matrix alignment methods allowing direct prediction of peptide MHC binding sequences and affinities were used to assess the two Ole e 11 protein isoforms for putative T-cell epitopes prediction. These included: TEPITOPE (www.bioinformation.net/ted), Propred (www.imtech.res.in/raghava/propred) (using quantitative matrices), NetMHCII (www.cbs.dtu.dk), Multipred (antigen.i2r.a-star.edu.sg/multipred), CTLpred (www.imtech.res.in/raghava/ctlpred) (artificial neural network approach), and RANKPEP (bio.dfci.harvard.edu/Tools/rankpep.html) (Position-specific scoring matrix), which employ binding status scoring qualitative prediction methods. HLA class II binding peptides of Ole e 11 were also predicted by calculating the inhibitory concentration (IC50)

value based in the following quantitative prediction methods: MHCpred (www.ddg-pharmfac.net/mhcpred/MHCPred), SVRMHC (SVRMHC.umn.edu/SVRMHCdb), ARB matrix methods (www.epitope.liai.org:8080/matrix), and SMM-Align in MetaMHC (www.biokdd.fudan.edu.cn/Service/MetaMHCII/server.html). Promiscuous peptides binding to multiple HLA class II molecules were selected.

The B- and T-cell epitopes identified by computational tools were mapped onto linear sequence and on the three dimensional model of Ole e 11 to determine their position and secondary structure elements involved.

Results

Olive PME sequences analysis

Ole e 11 belongs to the pectate lyase-like superfamily (InterProt number IPR012334, SCOP number 51126), and PME family (Gene Ontology number, GO: 0030599, SCOP number 51147). After searching for the characteristic motifs/patterns, Ole e 11 exhibited a unique pectin esterase pattern PS00503 ^{215}IeGTVDFIFG^{224}, located in the active (ligand-binding) site, in comparison with those PMEs from carrot, potato or tobacco, that contain an additional motif pectin esterase PS00800 ^{33}SktryviRIKaGVYREnvdV^{52} (Fig. 1).

Search of the corresponding databases (Allergome, www.allergome.org; and SDAP, fermi.utmb.edu/SDAP) for plant PMEs identified as allergens, resulted in the sequences of Act d 7 (*Actinidia deliciosa*), Ole e 11 (*Olea europaea* L.), Sal k 1 (*Salsola kali*), and Lyc e PME (*Solanum lycopersicum*). Sequences alignment of a representative number of plants PMEs analyzed in this work showed a wide range (54.8-5.6 %) of identity among them. We found a low identity when comparing olive to food PMEs such as kiwi (19.3 %), carrot (17.6-17.4 %), orange (14.4-11.8 %), potato (12.9-12.2), and tomato (12.7-11.8 %), or algae like *Phycomitrella patens* (19.5-14.9 %). The higher identities were those of *Arabidopsis thaliana* (54.7-50.2 %), and *Salsola kali* (52.3-51.7 %) pollen.

Previous sequence comparisons of several mature PME enzymes [19], have only shown six strictly conserved residues: G44, corresponding to G101 in the alignment of the Fig. 1, G154 (G217), D157 (D220), G161 (G224), R225 (R288) and W227 (W290). The residues are also conserved in olive PME isoforms, as well as several others highly-conserved aromatic residues, such as 4 F, 2Y, 2 W and 4P in our alignment. Furthermore, the alignment of amino acid sequences also showed five characteristic domains of PMEs with functional importance [19], which are not fully conserved in all olive PMEs: ^{102}GxYxE^{106}, ^{176}QA(V/**A**)AL^{180}, ^{198}QDTL^{201}, ^{220}DFIFG^{224}, and ^{286}LGR(P/**S**)W^{290} (Fig. 1).

The analysis of physicochemical parameters of allergenic PMEs (Table S1) displayed a molecular weight range from 60500.3 Da to 35367.8 Da, and an isoelectric point from 6.33 to 8.73 (Table S1). This Ip has shown to be basic in general for most of allergenic PMEs; neutral for the olive isoforms, and slightly acidic for kiwi and one isoform of tomato. All sequences exhibited a hydrophilic character, as indicated by the negative average value (-0.1633±0.1016) of the Grand index (GRAVY). PME sequences could be considered as stable proteins based on their average aliphatic index value of 83.683±7.097, and their average stability index (28.971±5.456), as per values lower than 40 are considered stable protein (Table S1).

Potential post-translational motifs implicated in the protein functional regulation were analyzed (Table S2). Polymorphism was predicted for more than 25 potential N-myristoylation motifs with a variable number of post-translational sites between 4 and 6, and a motif of amidation [dGKR] only present in the pollen PME sequences of olive and *Salsola kali* PMEs. Additionally, variability was detected in the number of glycosylation motifs, present in 11 different sites (1 to 4 per specie). Ten different types of kinases were predicted to potentially phosphorylate the PME sequences analyzed. Fruit PMEs were predicted to be more susceptible to phosphorylation by different types of kinases (Table S2) than pollen PMEs. Furthermore, a variable number of putative phosphorylation sites by multiple enzymes were found in all the sequences analyzed (Table S3). These include serine, threonine and tyrosine residues. The number of serine residues that is susceptible to phosphorylation ranged between 1-8, 1-4, and 3-6 for threonine, serine and tyrosine, respectively.

Phylogenetic analysis of pollen PMEs

Phylogenetic analysis was performed in order to determine the relationships between pollen PME sequences across species, including allergenic species (Fig. 2). Twenty-three sequences from pollen were aligned and clustering analyzed. The data clearly reveal four established groups/clusters. First group contained the olive PME sequences together with the *Salsola kali*. Sequences from *Arabidopsis* were represented in the four groups. Carrot, maize and *Arabidopsis* are clustered in group 2. Selected members of *Petunia*, *Medicago*, *Arabidopsis* and *Nicotiana* constituted the group 3, whereas members of *Arabidopsis* and *Brassica* constitute group 4.

Structural analysis of PMEs: 2-D elements prediction

Secondary structure prediction with SSpro8 server identified 8 and 7 α-helices and 20 and 19 β-sheets in Ole e 11-1 and Ole e 11-2, respectively. Alternatively, PredictProtein, and NetSurfP v1.1 predicted 7 and 5 α-helices for Ole e 11-1, 8 and 5 α-helices for Ole e 11-2, 19 and 18 β-sheets for Ole e 11-1, and 20 and 18 β-sheets for Ole e 11-2.

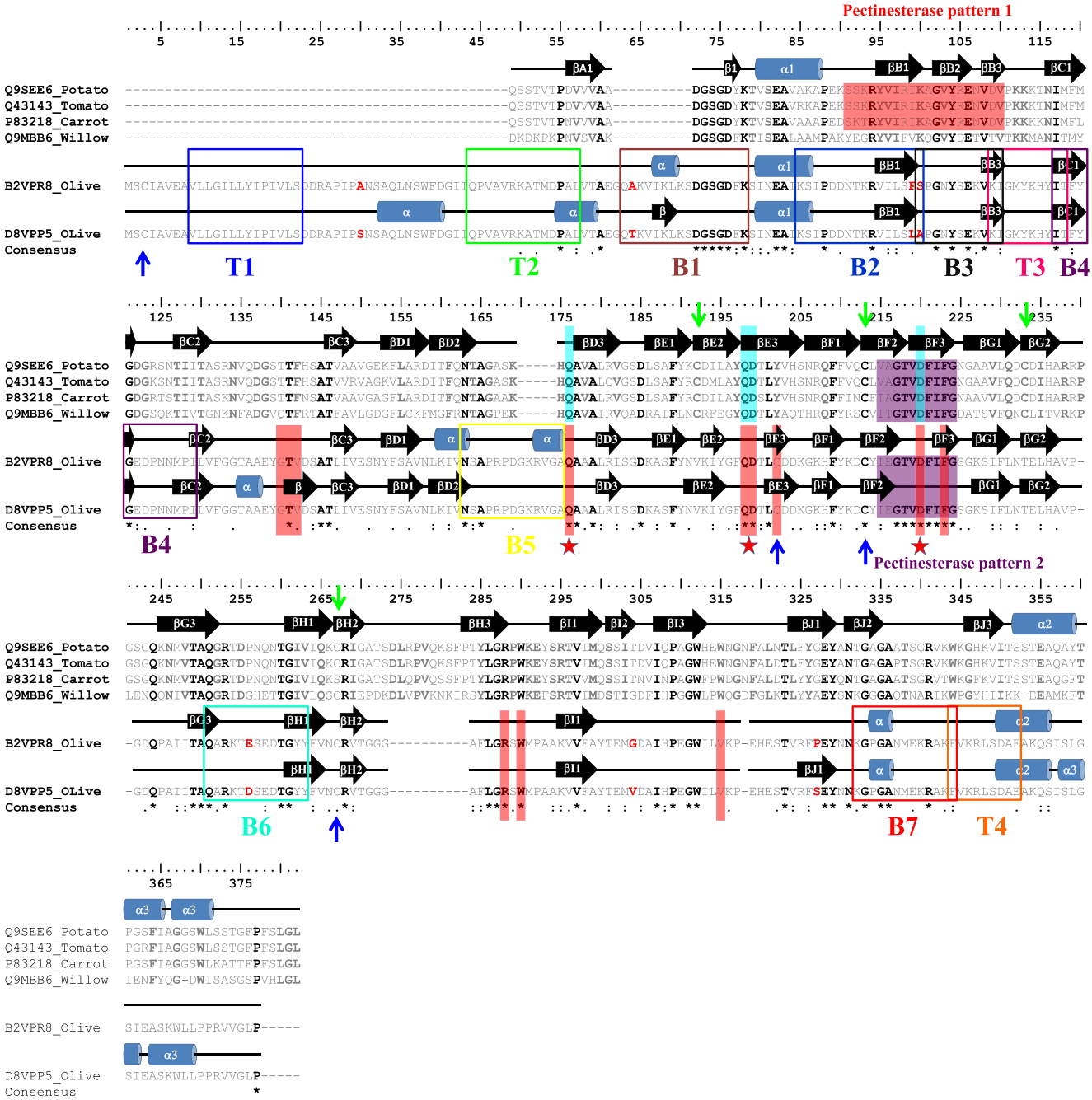

Fig. 1 Sequences and 2-D structure analysis of PMEs from different plant species. Sequence comparison of different plant PMEs (potato, Q9SEE6; tomato, Q43143; carrot, P83218; willow, Q9MBB6; and olive, D8VPP5 and B2VPR8) performed by multiple alignment. Residues conserved among the five species were highlighted black bold, while these only conserved in the four first species were highlighted gray bold. Cysteine residues were pointed out with blue arrows for olive and green arrows for the rest of the species. Variable amino acids in olive PME sequences were highlighted in red color. 2-D elements were depicted as barrels (α-helices) and black arrows (β-sheets). Pectin methylesterases patterns are highlighted by different colors. Residues implicated in the active center are shadowed by red and blue color for olive and other species, respectively. The amino acids implicated in the enzyme reaction mechanism were highlighted by a red star. Sequences of the T- and B-cell epitopes are framed in different colors, and named T1- T4 and B1-B7, respectively

The α-helical regions and β-sheets recognized by PSIPRED (8 and 21 for Ole e 11-1, and 6 and 20 for Ole e 11-2) were superimposed over the 3D structure of Ole e 11 (Fig. 1). Predictions made by the different servers correlated well with the modeled 3D structures.

Searching for templates

The search for the proteins PMEs with known tertiary structure in the Protein Data Bank (PDB) yielded carrot and tomato PMEs (PDB accession number 1gq8 and 1xg2,

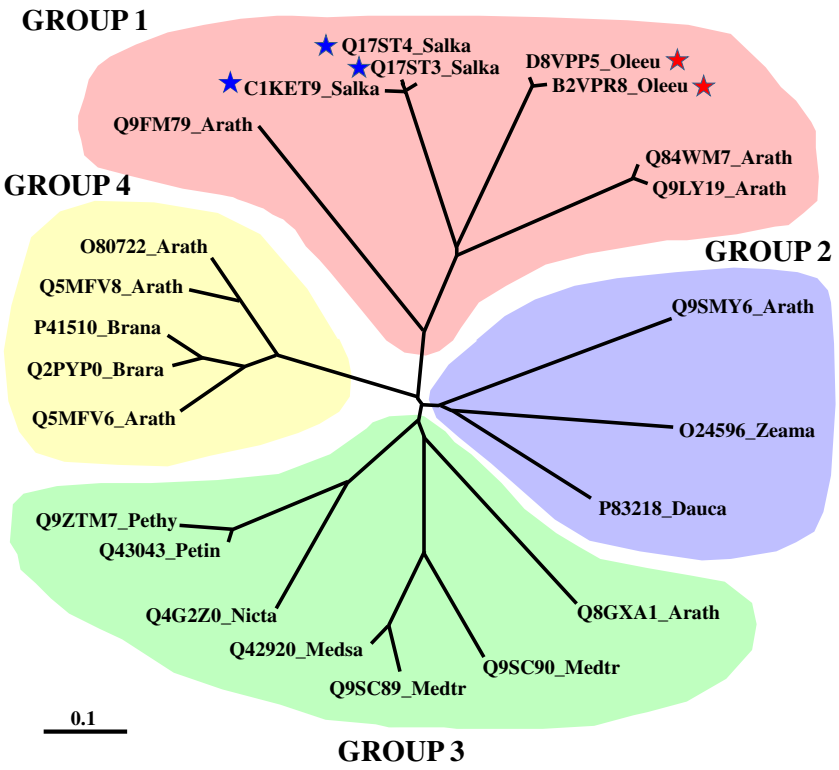

Fig. 2 Phylogenetic analysis of pollen PMEs. Neighbor-joining (NJ) method was used to perform a phylogenetic analysis of 23 pollen PMEs from *Arabidopsis thaliana* (Arath), *Brasica napus* (Brana), *Daucus carota* (Dauca), *Medicago sativa* (Medsa), *Medicago truncatula* (Medtr), *Olea europaea* L. (Oleeu), *Petunia hybrid* (Pethy), *Petunia indica* (Petin), *Nicotiana tabacum* (Nicta), *Salsola kali* (Salka), and *Zea mays* (Zeama). Four well defined groups were identified and highlighted by red, green, blue and yellow color respectively, group 1 is integrated by the olive PMEs isoforms (highlighted by a red star), and another three pollen protein isoforms already identified as allergenic PMEs from *Salsola kali* (Sal k 1, C1KET9, Q17ST3, and Q17ST4)

respectively) showing the highest sequence identity (22.2 and 21.8 % with Ole e 11-1, and 21.9 and 22.1 % with Ole e 11-2, respectively). The suitability of selected model was checked by BioInfoBank Metaserver, which returned 3D Jury scores (Jscore) of 209.75 (carrot) and 207.75 (tomato) for Ole e 11-1, and 209.25 (carrot) and 207.50 (tomato) for Ole e 11-2, respectively. The crystal structures of carrot and tomato PMEs were retrieved from PDB based on the above values. We also used the Swiss-Model server to check the best possible template to build the Ole e 11 structure, finding high scores (97, 96, and 94, respectively) and very low E-values (2E-20, 3E-20, and 1E-19, respectively) for the following templates that were also retrieved from PDB database and used for homology modeling: 1qjv (*Erwinia chrysanthemi*), 2ntp and 2nsp (*Dickeya dadantii*).

Quality of olive PMEs models

Different tools have been used to assess the quality of the models built for this study:

a) *Procheck analysis*. The main chain conformations of the protein models for Ole e 11-1 and Ole e 11-2 were located in the acceptable regions of the Ramachandran plot. A majority of residues (82.4 and 82.9 %, respectively) were in the most favorable regions, whereas 15.6 and 15.4 % of the residues were placed in the allowed regions, and 1.7 and 1.2 % were in generously allowed regions. On the contrary, only 0.3 and 0.5 % of the residues were present in the disallowed regions, respectively. The plot of x1 versus x2 torsion angles for each residue showed that most of the rotamers in Ole e 11-1 and Ole e 11-2 models were localized in low energy regions. The analysis of the same values for the crystal structures 1gq8 and 1xg2 from carrot and tomato PMEs showed 86.8 and 91.4 % of the residues in the most favorable regions, 11.7 and 8.4 % for allowed regions and 1.5 and 0.2 % for generously allowed regions, respectively. No residues were located in disallowed regions.

b) *ProSa analysis* returned Z-scores of -7.97 and -8.23 for Ole e 11-1 and Ole e 11-2, respectively. The scores were within the range usually found for native PMEs proteins of similar size, i.e., -7.41 for 1gq8, or -7.35 for 1xg2 crystal structures, respectively.

c) *ERRAT analysis*. Overall quality factors of 80.743 % and 79.234 % were assigned by Errat for Ole e 11-1 and Ole e 11-2 models, respectively, while A quality factor of 82.609 % and 93.318 % were assigned to the similar PMEs 1gq8 and 1xg2 crystal structures, respectively.

d) *QMEAN analysis*. Q values for Ole e 11-1 and Ole e 11-2 models were 0.676 and 0.675, respectively. A quality factor of 0.844 and 0.731 were estimated for the crystal structures 1gq8 and 1xg2, respectively.

e) Root mean square deviation (RMSD0 between Ole e 11-1 and Ole e 11-2 models and the crystal template Cα backbone of 1gq8 was 0.369 Å and 0.373 Å, respectively. RMSD between 1xg2 crystal template and olive

PMEs isoforms 1 and 2 was 0.657 Å and 0.659 Å, respectively.

The parameters followed to assess the quality of the olive PMEs models were equally checked for other PME models showing comparable values.

Three-dimensional structure of olive PME isoforms

The 3D structure of olive PME appeared to be a carboxylate hydrolase with a general topology similarly found in other pectinases, which includes two Asp residues (D199, and D220) at the active site [20]. Despite the low amino acid sequence identity across species, a relatively good conservation of the overall fold (Cα carbon chain) of this protein was found among plant species (Fig. 3, Fig. S1, Table S4, and Table S5).

We obtained the best structural models of the olive PME isoforms, based on homology modeling (Fig. 3). Both structures showed a high similarity in the overall folding, which was further confirmed by calculating the small RMSDs, after comparing Cα carbons superimposition of both pollen and fruits PMEs structures (Table S4). The general fold was also quite similar in PMEs from non-allergenic plant species (Fig. S1, Table S5).

Olive PME structures were characterized as right-handed parallel α-helix structure consisting of three parallel β-sheets (PB1, PB2 and PB3) with interconnecting loops (T1, T2 and T3) projected from the helix core (Fig. 3a), which is in accordance with the general crystal structure of carrot 1gq8. The environment inside the α-helix structure is essentially hydrophobic. Comparison between both olive isoforms did not exhibited large differences in the general topology as it was further confirmed by the RMSD value of 0.485 Å, whereas significant differences were found in particular regions of the proteins such as the N-terminal region, C-terminal loops, as well as the T3 loop and the small size of the PB2 β-sheet. These differences have been highlighted in Fig. 3a with arrows.

Olive PMEs showed four cysteines (Fig. 1). Two of them were found in the same position as in the sequences of carrot or potato PMEs (C203 and C267). Another cysteine was localized in the N-terminal region, where the presence of a putative signal peptide was predicted. The fourth cysteine was placed in the ligand-binding cleft. Individual comparison between olive isoforms and other allergenic PME isoforms from pollen and fruit (Fig. 3b) reveals major differences, which were located basically in the same secondary structural elements, the C-terminal regions, and spacial distribution of different loops. Furthermore, structural comparison between allergenic pollen PME isoforms (*Olea europaea* L. and *Salsola kali*) (Fig. 3c) showed differences in C-terminal region, the spacial distribution of different external loops, and in a sort PB2 structure.

Comparison between olive PMEs isoforms with fruit PME isoforms from kiwi and tomato (Fig. 3d) showed differences in the C-terminal region, and in the spatial distribution of different structural loops. Similar overall folding topology among pollen and fruit PMEs was confirmed by RMSD (Table S4). Finally, comparison between olive PME isoforms and non allergenic plant PMEs (Fig. S1), showed the same differences previously observed. Overall fold topologies were quite similar, as confirmed by the low RMSD calculated (Table S5).

Proteins surface, electrostatic potential and conservational analysis of olive PMEs

The surface structures in both Ole e 11 isoforms were similar (Fig. 4). Surface of Ole e 11-1 (rotated 180°) showing the secondary structure elements (embedded inside) was depicted in Fig. 4a. The morphology of the cavity that accommodates part of the pectin chain is situated in a solvent-accessible cleft across the molecule formed by the external loops (Figs. 3a, 4a and b). The central part of this cleft is lined by several aromatic residues (Fig. 1), a characteristic feature for most carbohydrate binding sites. The putative active (ligand-binding) site is located on the PB3 sheet, and contains the amino acids G140, T141, V142, Q176, Q198, D199, C202, D220, F223, R276, W278, V303, where several of them are well conserved (Q176, Q198, D199, D220, R276) (Fig. S1). Olive PMEs, as those from other plant species such carrot and/or tomato, differ from the bacterial PMEs at the substrate-binding cleft, by having less-pronounced walls. Bacterial PME active site walls are higher due to the presence of much longer loops [21].

Surface electrostatic potential analysis (Figs. 4b, 5c) reveals several prominent charged residues, with half of the side exhibiting large positive values (blue regions), and the other half showing predominantly negative values (red regions) (Figs. 4b, 5c). By assigning a value of +1 to basic residues (H, R, K) and -1 to the acidic residues (D, E), net charge of protein was calculated to be +5 for both Ole e 11-1 and Ole e 11-2. The cavity holding the pectin chain exhibited a predominantly negative charge.

Consurf conservation analysis showed that PMEs are not conserved, especially these residues located in the surface of the protein (Fig. 4c). This is in accordance with the calculated low identity of the amino acid sequence, as well as with the multiple alignment comparison between plant species. The most conserved region of the protein is the central area of the ligand-binding cavity (see magnification in the Fig. 4c and d), and other amino acids with a major role in the maintenance of the protein structure. A clear distribution of the conserved (purple) and variable (turquoise) residues can be appreciated in the core and the surface (N- and C-terminal and loops) of the protein, respectively (Fig. 4d). This distribution of variable and conserved residues helps

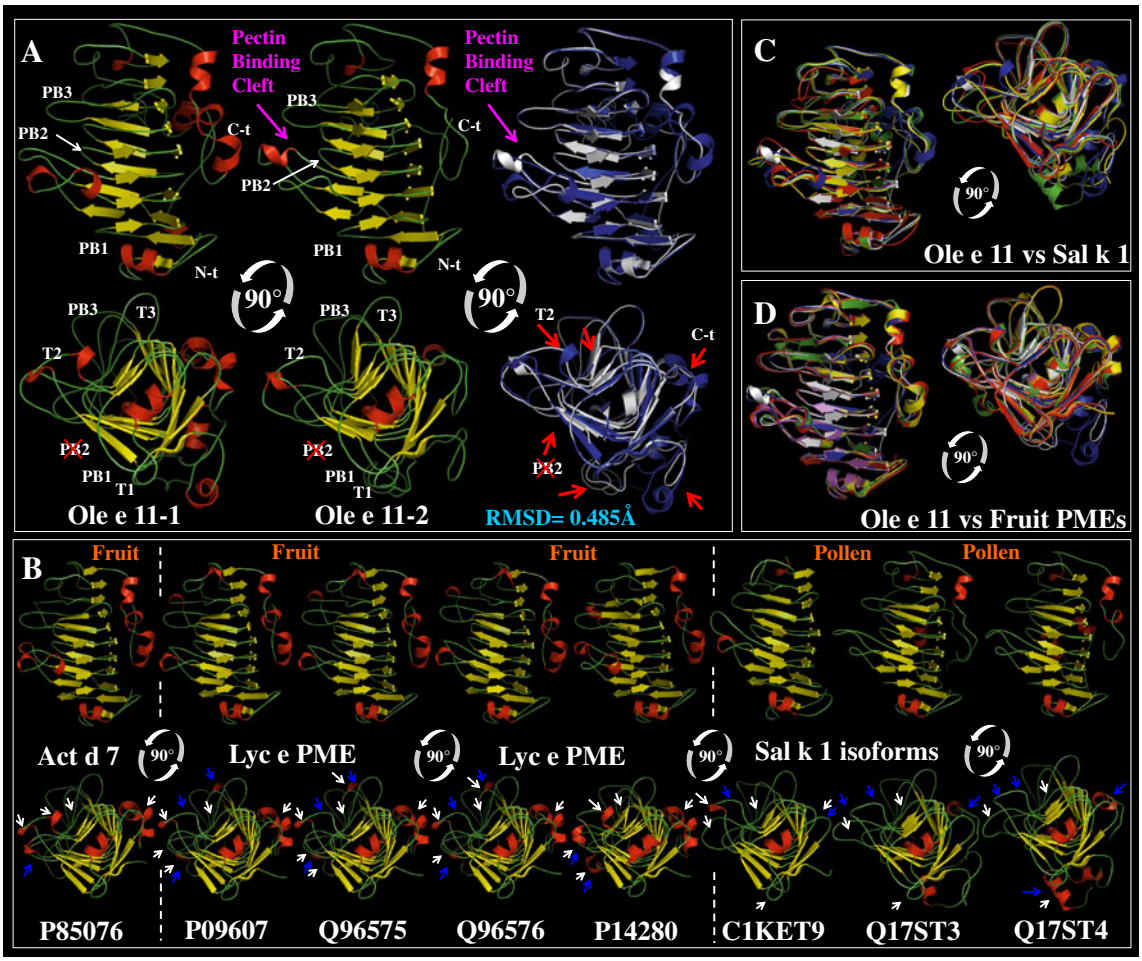

Fig. 3 Three-dimensional structure analysis of allergenic plant PMEs. All structures were depicted as a cartoon diagram. α-helices, β-sheets and coils are depicted in red, yellow and green respectively. Two views (rotated 90 around the x-axis, looking down from the N-terminal side) are provided for each model. (**a**) Three-dimensional structure of olive pollen PME isoforms D8VPP5 (Ole e 11-1) and B2VPR8 (Ole e 11-2). Different secondary structural elements are highlighted as three parallel β-sheets PB1, PB2 and PB3. Loops forming the pectin binding cleft, as well as loops T1, T2 and T3 between sheets are also indicated. Superimposition between both olive pollen PME isoforms is depicted in blue (Ole e 11-1) and white (Ole e 11-2) color. Structural differences between both isoforms are highlighted with red arrows. (**b**) Three-dimensional structures of allergenic PMEs like pollen Sal k 1 (three isoforms), or fruit PMEs like Act d 7 and four different isoforms from tomato (P09607, Q96575, Q96576 and P14280) are displayed. Structural differences (presence or absence of the 2-D structural elements) compared to Ole e 11-1 and Ole e 11-2 are highlighted with blue and white arrows. (**c**) Comparisons of pollen PME structures performed by superimpositions. Ole e 11-1, Ole e 11-2, and Sal k 1 (C1KET9, Q17ST3, and Q17ST4) are depicted in blue, white, red, yellow, and green colors, respectively. (**d**) Comparisons of olive PMEs and fruit structures performed by superimpositions. Ole e 11-1, Ole e 11-2, Act d 7, Lyc e PME (P09607, P14280, Q96575, and Q96576) are depicted in blue, white, red, yellow, orange, and magenta, respectively

maintain a similar overall fold among plant PMEs, but also produces differences observed in the spacial distribution and length of different structural elements as loops as the result.

The ligand-binding site and the catalytic activity of olive PMEs

The putative active site in olive PME is located at a cleft (on the PB3 sheet) and contains several conserved amino-acid residues: two aspartate residues (D199, and D220), which are distinguishable features of aspartyl esterases, two Gln (Q176, Q198) and one Arg (R276). The pectin chain substrate bound to the cleft is depicted in the Fig. 5a. These essential amino acids for the catalytic activities of the enzyme are well conserved (Figs. 1, 5d). Figure 5b and c show the long cleft across the PME structure, with a rotation of 45° with respect to the y-axis, having all the properties expected for the pectin binding site, including a central part integrated by several aromatic residues (Fig. 1), which is a characteristic for carbohydrate binding sites; i.e., V142, C202, F223, F285, W278, F300, and V302. The interactions between the pectin polymer and the long substrate cleft with its aromatic rings should be sufficient to keep the substrate bound to the enzyme for additional cycles of catalysis. Figure 5e shows a general view of the amino acids in the cavity holding up the molecule of methyl-α-D-

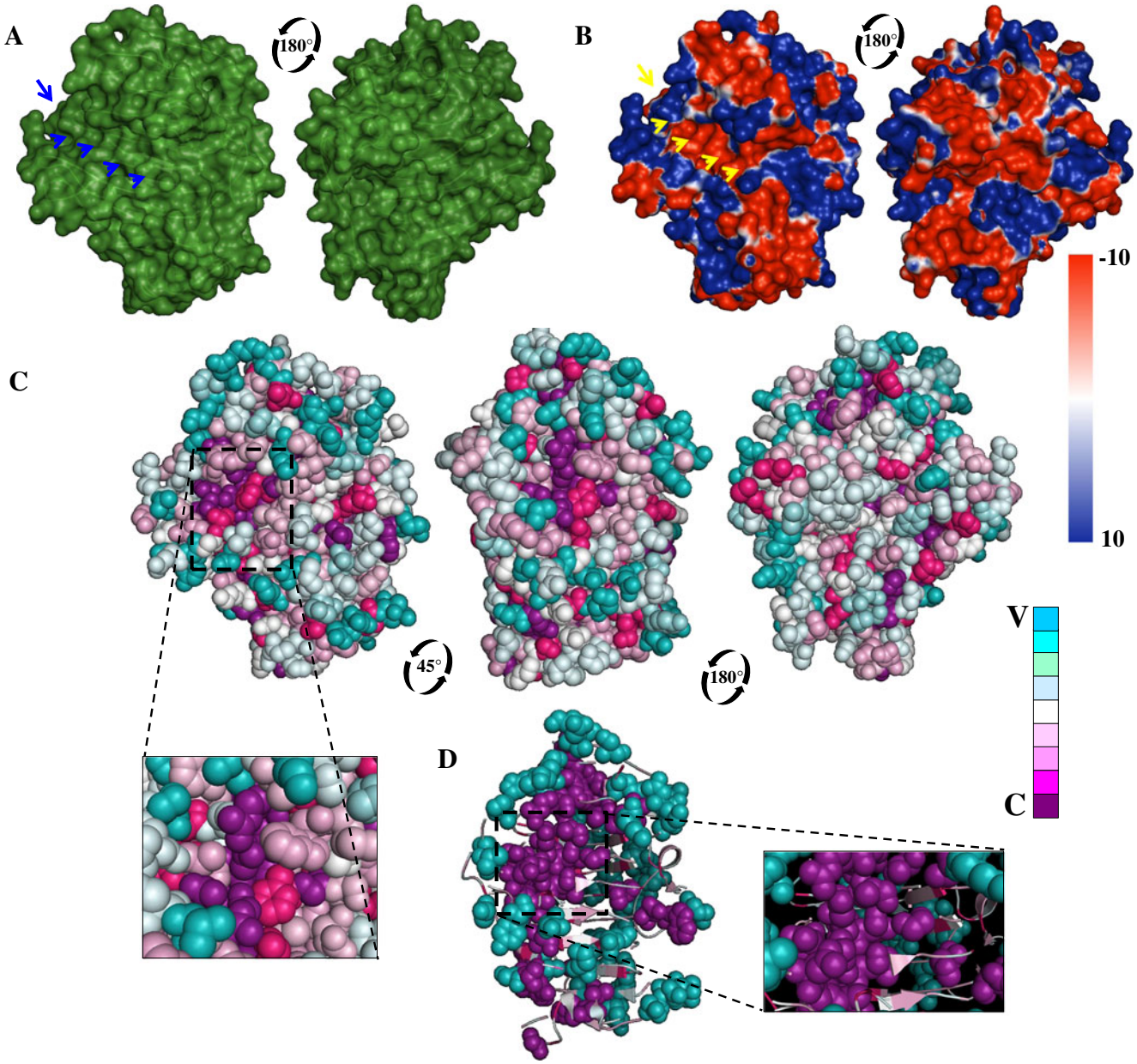

Fig. 4 Olive PME surface structure, electrostatic potential and conservational analysis. (**a**) Surface representation views of the Ole e 11 rotated 180°, showing the pectin chain binding cleft highlighted by blue arrows. (**b**) 180° rotated views of the electrostatic potential representation on the Ole e 11 protein surface, showing the pectin chain binding cleft highlighted by yellow arrows. The surface colors are clamped at red (-10) or blue (+10). (**c**) Consurf-conservational analysis of the Ole e 11 protein showed in three individual views rotated 45 and 180° respectively. The conserved and variable residues are presented as space-filled models and colored according to the conservation scores. A detailed view of the cavity with the active center is shown in high magnification. (**d**) A detailed view of the Ole e 11 protein showing the distribution of the strictly conserved (purple) and variable (blue) residues. The active center is shown in high magnification. C=conserved, V=variable

galactopyranuronate (MGAP). A detailed view of the catalytic domain shows the spacial distribution of the R-chain of every amino acid responsible for the conformation of the ligand binding domain surrounding the MGAP residue. Conformation predictions indicate that the methyl- groups integrating the glucuronan chain of pectin is projected to the inside of the cavity.

PME inhibitory interaction mechanism: docking analysis with a homologous inhibitor

In order to get insights about PME physiology and regulation by PMEIs in plants, as well as the possible applications and implications in the food-industrial biotechnological processes, we have analyzed the conformational interaction between

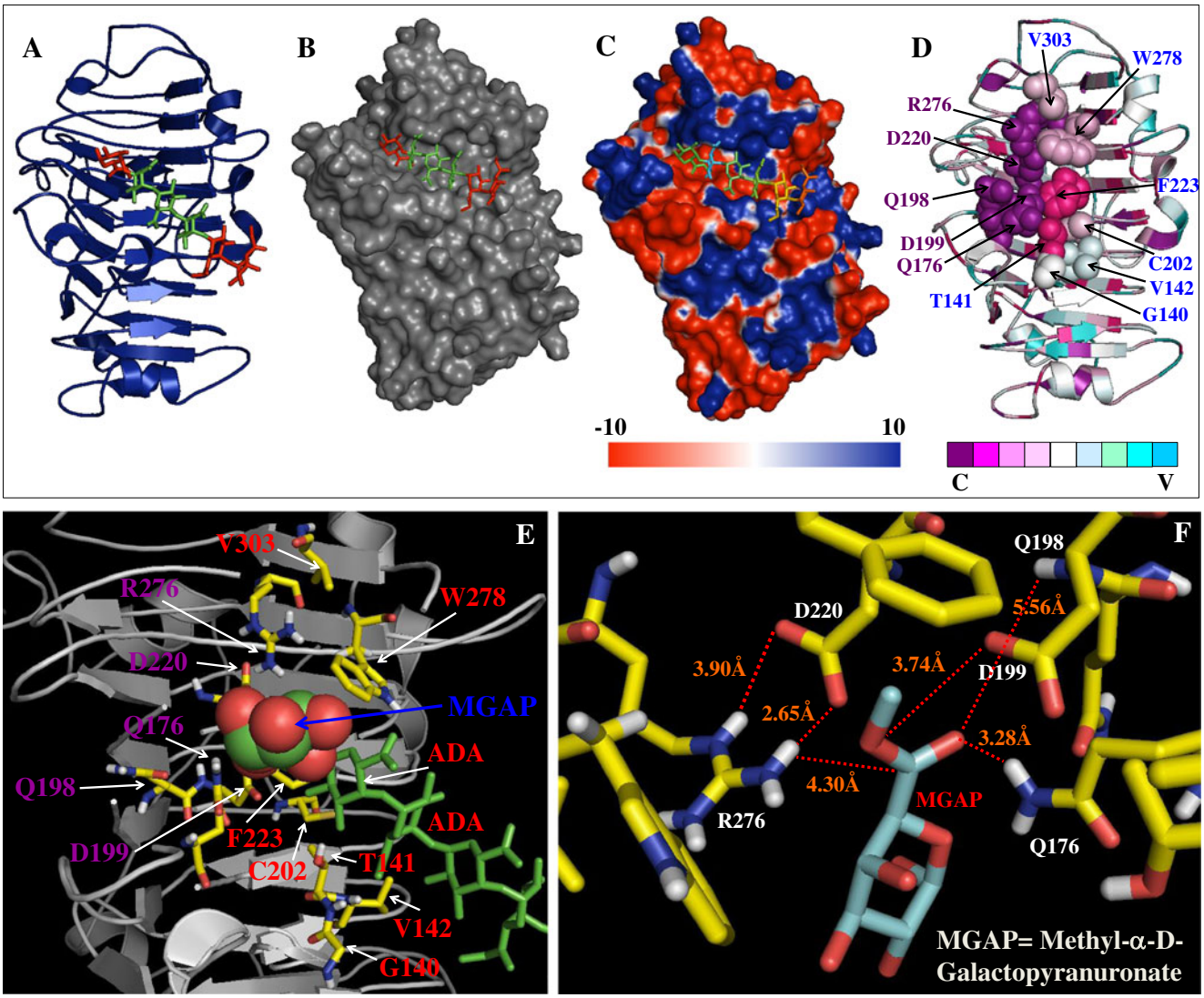

Fig. 5 Ligand-binding domain analysis. (**a**) Blue cartoon representation of Ole e 11-1 showing the ligand (pectin chain) binding domain. Ligand residues of methyl-α-D-galactopyranuronate (MGAP) are colored in red, while α-D-galactopyranuronic acid (ADA) residues are depicted in green color. (**b**) Surface representation of the pectin binding cleft in gray color showing the pectin chain lining on the cleft binding surface. Loops from T2 and T3 form the walls of a cleft running across the molecule. Aromatic residues are lining the cleft, as seen in other carbohydrate binding proteins. (**c**) The Poisson–Boltzmann electrostatic potential representation of the pectin binding cleft. Pectin chain is depicted in rainbow color. (**d**) Conservation analysis of the residues directly implicated in the pectin chain interaction (G140, T141, V142, Q176, Q198, D199, C202, D220, F223, R276, W278, V303). It is noticeable that residues involved in the de-esterification mechanism (Q176, Q198, D199, D220, and R276) are well conserved. (**e**) Detailed view of the pectin chain and the spatial distribution of the interacting residues. Residues are depicted as stick and colored according with atoms. (**f**) The active site, where a molecule of substrate, methyl-esterified D-galacturonic acid is modeled. The five catalytically important residues (Gln176, Gln198, Asp199, Asp220 and Arg276) are depicted in the same way as that in the previous section. Inter-atomic distances were calculated in Armstrong units, highlighted with discontinued red lines. Arg276 is hydrogen-bonded to Asp220, which is properly placed for nucleophilic attack on the carboxymethyl carbon, while Asp199 would act as an acid/base during catalysis. The two glutamine residues, Gln1176 and Gln1198, could form an anion cavity for stabilization of the negatively charged tetrahedral intermediate

olive PME and a proteinaceous inhibitor (PMEI) partner. For this purpose, the sequence of a carrot PMEI was used (Fig. 6) as heterologous sequence since olive are lacking. This analysis was carried out by molecular docking, using newly modeled structures of both interacting partners. Moreover, we have chosen the inhibitor from carrot due to the structural close-relationship between olive and carrot PMEs.

Figure 6a shows the mode of interaction between olive PME and carrot PMEI. The inhibitory mechanism occurs through the formation of a non-active complex (stoichiometry 1:1) between enzyme and inhibitor. A detailed view of this interaction is depicted in the magnifications displayed in Fig. 6b, where PMEI is located just over the cavity that holds the substrate methyl-α-D-galacturonate. PMEI covers

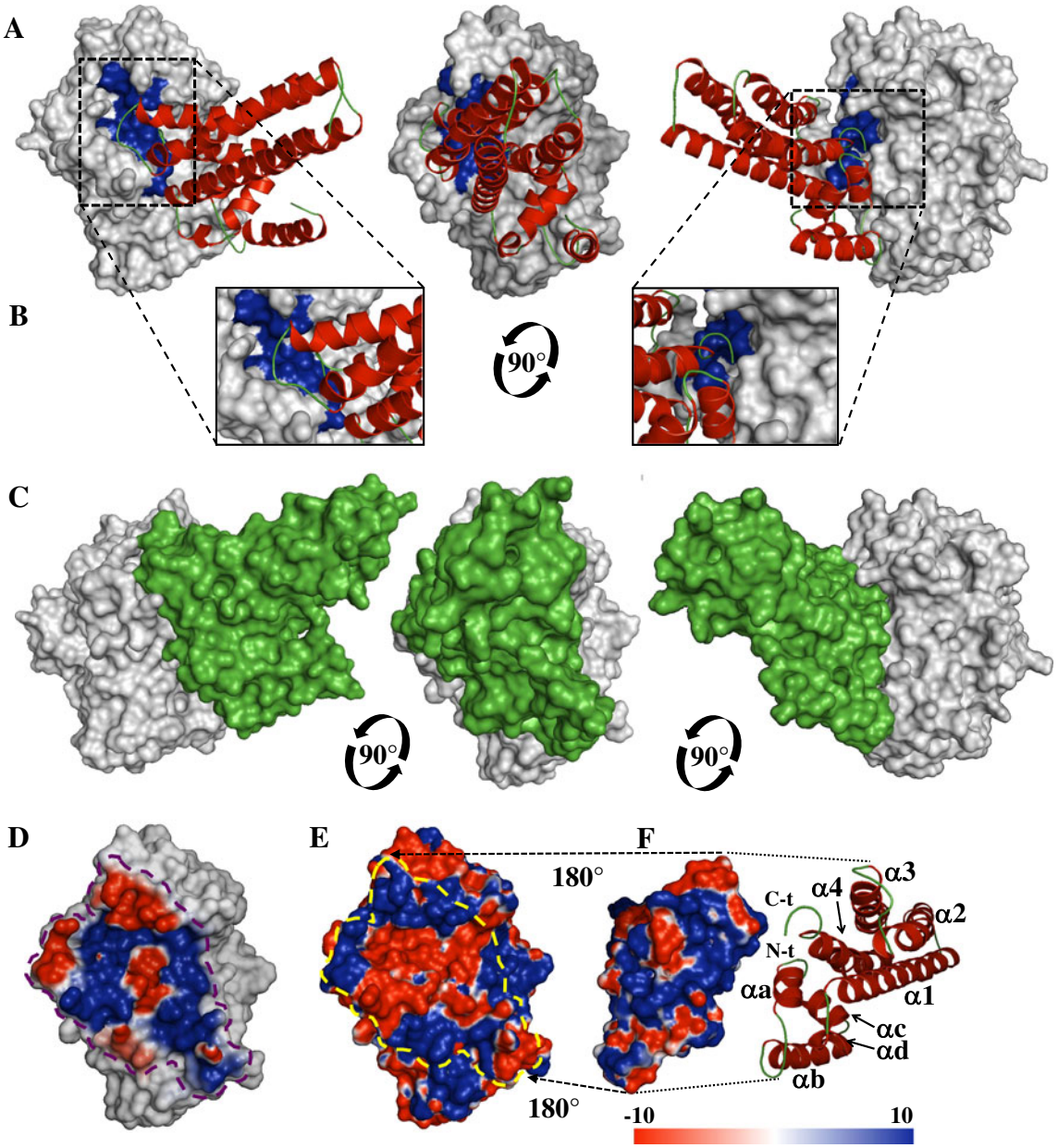

Fig. 6 Analysis of the interaction between olive PME and carrot PMEI proteins. (**a**) The complex between olive PME (gray surface representation) and carrot PMEI (red and green cartoon representation) were rotated 90°. (**b**) Detailed views of the ligand binding clef are depicted, where PME residues implicated in the ligand interaction are blue colored. (**c**) Surface structures rotated 90° in gray (olive PME) and green (carrot PMEI) are depicted, and highlight the large interacting surface between both proteins. (**d**) Contact fingerprint of the electrostatic potential of PMEI on the surface of the PME. (**e**) Electrostatic potential of the interacting area highlighted by a yellow discontinued line. The opposite charged areas depicted in D and E section matched well. (**f**) Electrostatic potential of the PMEI interacting face. Cartoon diagram showing the secondary structural elements of PMEI (αa, αb, αc, αd, α1, α2, α3 and α4)

completely the active (ligand-binding) cleft, therefore preventing the access of the substrate. It also impedes the interactions that are necessary for binding the rest of the pectin chain to the enzyme cleft [21]. The interaction is non-covalent, thus it should be reversible by increasing salt concentration and/or pH to alkaline conditions. Figure 6c shows the large area (≈1457Å^2) covered by the PMEI molecule in the PME.

In terms of energy, the electrostatic potential analysis for the contact surface of both PME and PMEI structures exhibited high compatibility in positive and negative interacting residues (Fig. 6d to f). There are not large areas with hydrophilic character in the contact surface between PME and PMEI, and the formation of the complex may be mediated by a high number of direct and water-mediated H-bonds.

Representation of the PMEI fingerprint of charges (electrostatic potential) on PME surface contact (Fig. 6d) showed a large number of residues with opposite charges in a compatible distribution with the charges displayed in the contact surface of PME (Fig. 6e). Figure 6f shows five different regions of the PMEI taking part of the contact surface: 1) N-t-αa; 2) helix αA-^{18}AAAsAAPAnqFI^{29}-helix αB; 3) helix αD-^{53}IqnnPq^{58}-helix α1; 4) helix α2-^{118}**K**nLs**H**A**K**Gn**D**FtF**R**^{131}-helix α3; and 5) helix α4-^{186}nFAA**KHKH**^{193}-C-terminal (polar residues are in low case and charged residues in bold).

In terms of structure, i) the N-terminal helical hairpin of PMEI does not or only slightly affects the interaction with olive PME, ii) the first loop between the αa and αb might be involved in the stabilization of the complex, iii) catalytically important residues are also implicated in making contact with the inhibitor, i.e., K190 in the C-terminus of the PMEI is implicated in the contact with both aspartate residues of the active center, D199 and D220, iv) aromatic residues of the carbohydrate binding cleft are involved in the stabilization of the interaction, v) the interaction blocks the pectin-binding cleft that impede the entrance of a new pectin chain, vi) the interaction is non-covalent and reversible by high salt and high pH conditions, with a stoichiometry 1:1, vii) non dramatical changes have been observed in the 3D structure for PME or PMEI upon complex formation, viii) posttranslational modifications such as N-glycosylation seem not to affect or even regulate the interaction of PME and PMEI, since pattern/motifs of glycosylation are located outside of the interacting area in olive and other species analyzed, despite the variability exhibited in the number and location of these motifs.

Identification of highly antigenic regions in olive PMEs

Physicochemical parameters such as hydrophilicity, flexibility, accessibility, turns, exposed surface, polarity and antigenic propensity of polypeptide chains have been correlated with the location of continuous epitopes. Hydrophobicity (or hydrophilicity) plots were designed to display the distribution of polar and apolar residues along a protein sequence. In this study, antigenicity determinants were targeted by locating the positive peaks in hydrophilicity plots, thus identifying the regions of maximum potential antigenicity (Fig. S2). Kyte-Doolitte scale was used to search hydrophobic regions in the proteins. Hopp-Woods scale was used for predicting potential antigenic sites of the protein (which is essentially a hydrophilic index with apolar residues assigned negative values) [22]. Welling antigenicity plot assigns an antigenicity value, defined as the log of the quotient between the percentage of antigenicity in a sample of known antigenic regions and in average proteins. Parker antigenicity method was also analyzed [23]. We identified up to eight regions in the sequences of Ole e 11 with high potential of antigenicity (Fig. S2), which correlated well with the T- and B-cell epitopes predicted by using different methodologies.

Prediction of T-cell epitopes

Different publicly available tools were employed for determination of HLA class II binding sequences. Four amino acid sequences (P8: 9-22, P9: 44-57, P10: 109-118, and P11: 344-352) (Fig. 1, Table S6) were identified as promiscuous binders. One of these epitopes was located in the N-terminal region, in the signal peptide sequence. The epitopes were located in highly antigenic regions (Fig. S2). The predicted epitopes were comprised of 46 residues with a high frequency of occurrence for valine (11 %) and leucine (13 %). Of the total residues 65 % were non polar, whereas 28 % were polar. Charged residues (22 %) were least preferred in the T-cell epitopes. All four T-cell epitopes are located in areas of the protein, in which the amino acids involved in the epitopes displayed a solvent accessibility greater than 30 % and 50 %. All four T-cell epitopes are primarily composed of β-sheets. The epitopes P8, P9, and P10 are localized close to the N-terminal region and P11 in the C-terminal area of the protein. Epitopes P10 and P11 showed five residues overlapping with two B-cell epitopes. Surface distribution of T-cell epitopes was superimposed in the structure Ole e 11-1 and depicted in Fig. 7.

Prediction of B-cell epitopes

Seven antigenic regions prone to B-cell binding were predicted in Ole e 11-1 and Ole e 11-2 (P1: 63-73, P2: 85-100, P3: 100-110, P4: 117-129, P5: 163-175, P6: 251-263, and 6: 332-344) (Table S6). All the B-cell epitopes were located on the surface of the protein molecule in Ole e 11-1 isoform. Lysine (13.7 %), proline (10.47 %), followed by glycine (9.5 %), and serine (9.5 %) were the most common residues in the epitopes. The hydrophobic content was analyzed in order to identify regions with a higher probability of interaction with immunoglobulin. Around 42 % of the 95 residues were non polar, 37.89 % were charged residues and 26.30 % were recorded as polar residues for the predicted epitopes. The relative surface accessibility values showed 42.60 % residues with solvent accessibility greater than 30 %, whereas 27.26 % residues presented values greater than 50 %.

Small differences were detected in Ole e 11-2 in comparison to Ole e 11-1, because of the variability of both sequences, i.e., epitopes P1: t to A; P2: LA to Fs; P3: A to s; and P6: D to E. The software used for the identification of conformational epitopes over the surface of the proteins have recognized residues of all the first seven peptides (Table S6) as suitable parts of surface discontinuous epitopes. Surface distribution of B-cell epitopes was superimposed in the structure Ole e 11-1 and depicted in Fig. 8.

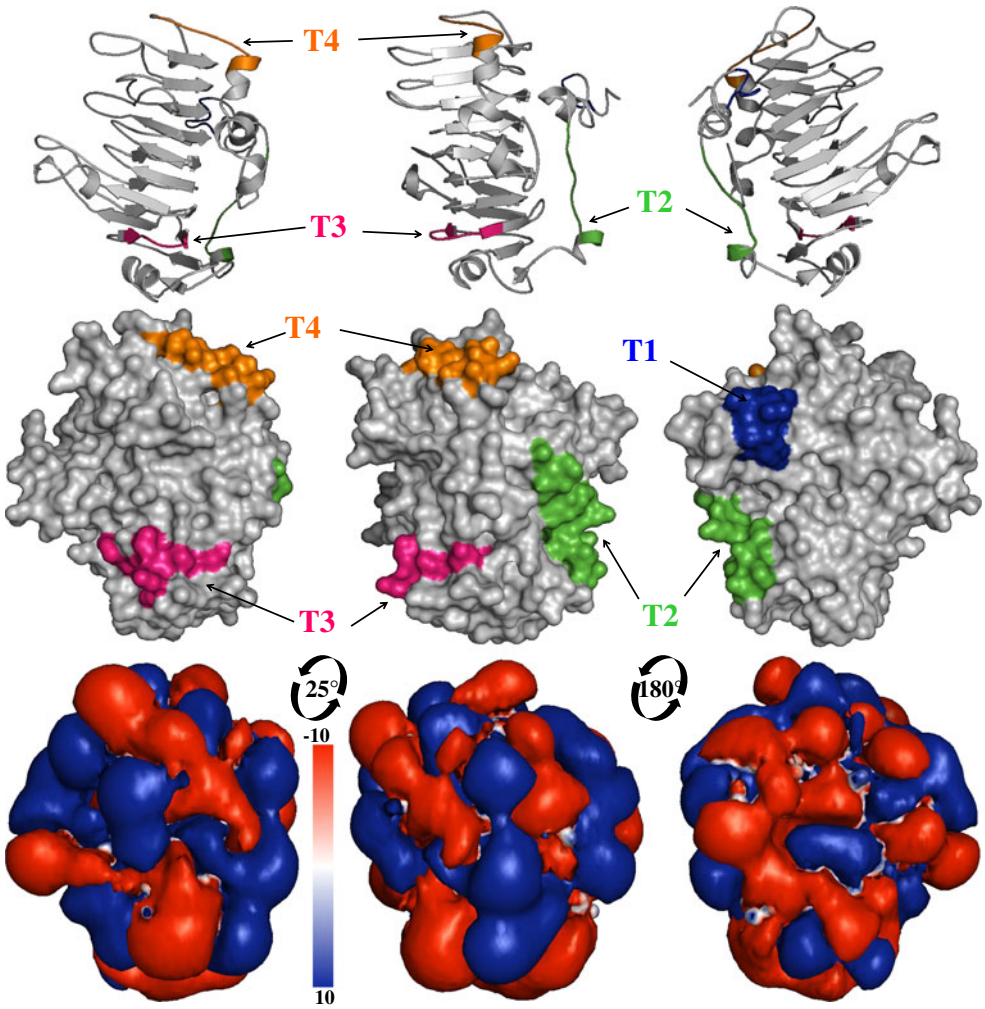

Fig. 7 T-cell epitopes superimposition on the surface of the Ole e 11 allergen structure. (**a**) Cartoon representation of Ole e 11 four views rotated 25° and 180° respectively, showing the localization of four epitopes (T1 to T4) in the 2D structural elements of the protein. All epitopes are integrated by final part of two α-helices and its corresponding flanking loop. T1, T2, T3, and T4 epitopes are depicted in blue, green, pink and orange colors. (**b**) T-cell epitopes depicted on the Ole e 11 protein surface following the same colors code than in previous section. (**c**) Electrostatic potential (isocontour value of ±10 kT/e) depicted in the Ole e 11 surface, showing the charge nature of the epitopes

Discussion

PME sequences and structural analysis revealed high variability implicated in isoforms generation

The presence of a large number of isovariants is one of the most distinctive properties in higher plants, particularly for PME family of proteins, despite the fact that all catalyze the same reaction [24]. The analysis of different physicochemical parameters in olive PMEs and comparison between pollen and fruit PMEs had shown a remarkable variability. The Ip of olive PME isoforms was in both cases close to the neutrality. Only a few studies have revealed the presence of acidic plant PMEs [25, 26], i.e., flax, mung bean, jelly fig, aspen and chicory root, ranging the Ip from 3.1 (fungal) to 11 (tomato). Most plant PMEs present neutral or alkaline Ips, which explain their tight association with the slightly acidic cell wall. Overall, plant PMEs and most bacterial PMEs and the fungal PMEs generally present more acidic Ips [25].

Sequence analysis of olive isoforms showed several micro-heterogeneities in different regions of the gene. Seven residues of the sequence were polymorphic, which variability was affecting different areas of the protein, i.e., 2-D structure elements, ligand-binding region, B-cell epitopes. In addition, few studies have described the high variability of PME with regard to numerous parameters including catalytic properties, optimal pH, salt dependence, substrate specificity and demethoxylation patterns [19]. Protein stability, molecular weight, multi-optional post-translational sites and functional motifs, i.e., N-myristoylation, absence or variable sites of amidation, number and type of N-glycosylation sites, and multi-optional motifs of serine/threonine or tyrosine phosphorylation implicated in protein regulation have been found in all PME proteins examined. These differences in PME isoforms might be reflected in the classification of PMEs into different groups in the clustering analysis, sharing common or differential functional-regulatory motifs.

Moreover, tissue-dependent PME properties are in agreement with the fact that isoforms vary depending on the developmental stage (e.g., fruit ripening, microsporogenesis, germination or stem elongation) [7, 19, 25], and the organ considered (e.g., flowers, fruits or roots) [7, 24]. These properties can be considered a major regulatory mechanism of endogenous plant PME activity [27, 28]. Expression of PME

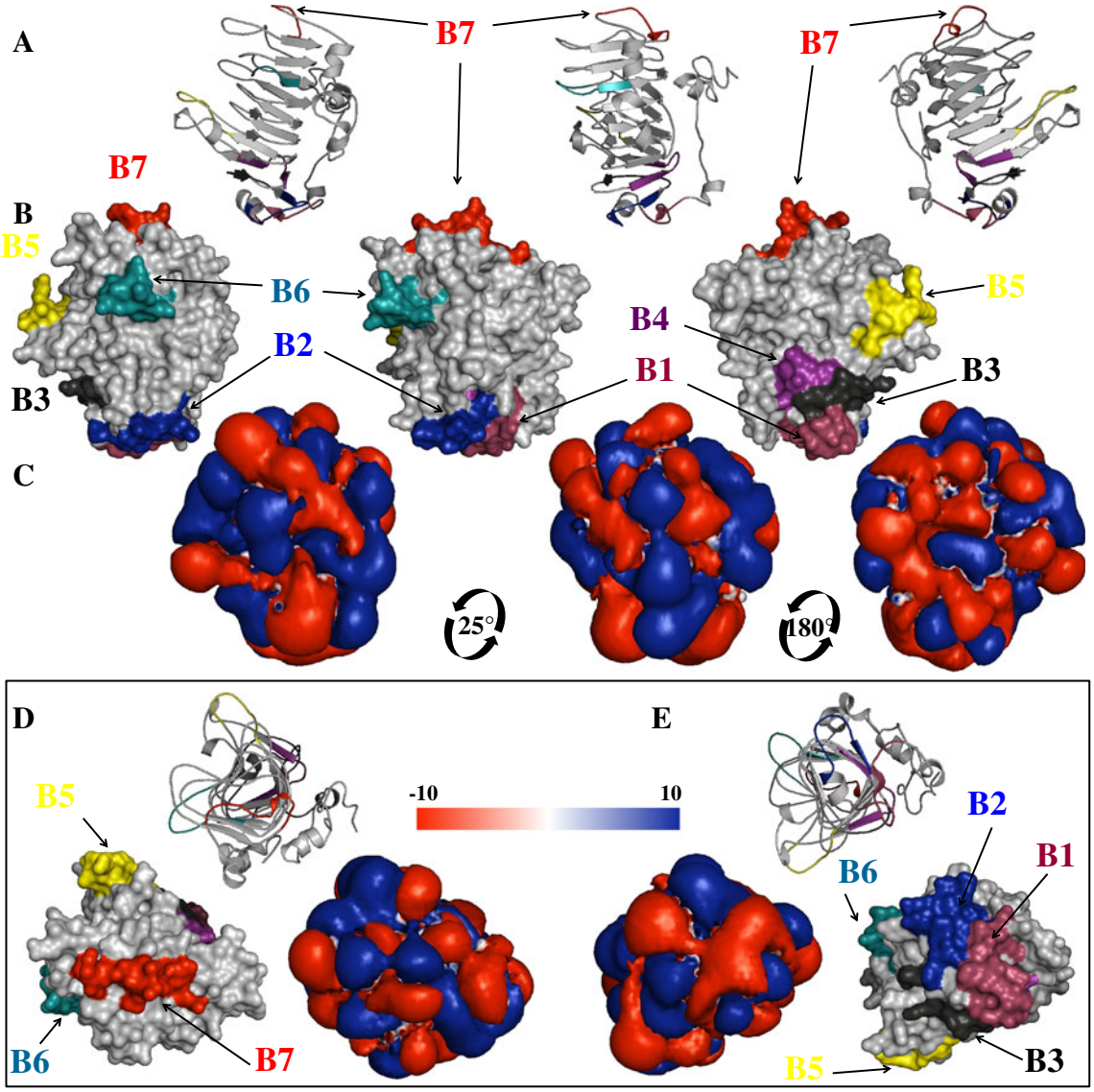

Fig. 8 B-cell epitopes superimposition on the surface of the Ole e 11 allergen structure. (**a**) Cartoon representation of Ole e 11 three views rotated 25° and 180° respectively, showing the localization of seven B-cell epitopes in the 2-D structural elements of the protein. Overall, the epitopes are integrated by the final part of one or two α-helices and its flanking loop. B1, B2, B3, B4, B5, B6, and B7 epitopes are depicted in light brown, blue, black, green, purple, yellow, tuques, and red colors. (**b**) B-cell epitopes depicted on the Ole e 11 protein surface following the same colors code than in previous section. (**c**) Electrostatic potential (isocontour value of ±10 kT/e) depicted in the Ole e 11 surface, showing the charge nature of the epitopes. (**d**) Cartoon, surface and electrostatic potential representation of a view of Ole e 11 protein rotated 90° around the x-axis, looking up and (**e**) down from the N-terminal side

isoforms has been described to display stress-specific patterns, depending on environmental changes [29]. Finally, the variability in the number of PME isoforms exhibiting common or differential functional and regulatory properties could increase even more, among the genetic background of plant species like olive, which germplasm includes more than 2000 cultivars around the world. This fact has been previously demonstrated for the major olive pollen allergen Ole e 1 [30], and the panallergen Ole e 2 [31].

Structural variability among PME isoforms might be an additional mechanism to generate functional variability, which also might explain to some extent the high number of PME isoforms found in different tissues, organisms, and in response to different stress conditions [29]. The conservational analysis further confirmed this observation, since most conserved residues in olive (present study) and other plant species [25] were located in the core of the structure. Surprisingly, a high variability was found in amino acids located in the surface of the protein, particularly in 2-D structural elements such as loops/turns. This variability might justify differences found for several characteristics such as length, spatial distribution of 2D elements and

changes in the electrostatic potential. Particularly, electrostatic potential represents an important property driving the interaction of PME with other protein partners for regulation and protein subcellular targeting [10, 28, 32]. The analysis of the 3D structure of the olive PMEs suggest that the protein fold has been strongly conserved among plant species, having deep implications for both functional and regulatory properties among isoforms as proposed for other olive allergen [30, 31].

Besides, the structural stability and interactive properties of PMEs might be influenced by the variability of the protein surface residues, since N-glycosylation motifs either N-linked or O-linked, seem to play a relevant role in the proper folding and stability of the PME isoforms. The analysis of N-glycosylation motifs in different species, including olive PME, has revealed large differences among isoforms, specifically in the number and surface distribution of glycosylation motifs. That distribution did not seem to affect the catalysis or ligand-binding regions as it was found previously for kiwi fruit PME [33]. This indicates that the enzyme may be differentially glycosylated, i.e., PME isoforms of kiwi fruit [34], thermally tolerant isoenzyme (TTPME) from orange [35], the acidic enzyme of jelly fig achenes [36], *Aspergillus* species [37], and PME of mung bean (*Vigna radiata*) hypocotyls. The distribution of the N-linked glycans suggests that they may stabilize the PME structure by shielding areas of the protein surface having lower hydrophilic character. On the other hand, N-linked glycans could also have a role in the protection of the polypeptide backbone from proteolytic degradation [33].

Cystine bridges are other differential element considered as critical part for maintenance of the structural integrity. These elements apparently do not play such critical role in PME protein structure maintenance, since a high variable number of cysteines and positions in the sequence can be found in many PME sequences [25]. Olive PMEs have four cysteines residues, one of them located in the N-terminal region where signal peptide is located, which may be lost later when the protein enters the secretory pathway. Furthermore, presence of two disulfide-bridged for the tomato PME main isoform (P14280) [38, 39] was described previously. The 3D structure of PME from *E. chrysanthemi* has approximately equal amounts (one) of disulfide stacked and disulfide-bridged forms (Cys150 and Cys170) [40], while in the 3D structure of carrot, no disulfide bridge exists, and the three cysteines (Cys129, Cys150 and Cys170) found in its sequence form an internal stacking ladder [41]. It should be possible to generalize that a non disulfide-bridge will be made in PMEs having three conserved Cys residues corresponding to those of carrot PME.

Comparative protein structure modeling is entirely a computational process that relies on the evolutionary relationship between the target and template proteins. Thus, the application of this approach is limited by 1) the availability of high-resolution experimental suitable template structures; 2) the ability of alignment methods to calculate an accurate alignment between the target and template sequences; 3) availability of refinement, assessment and evaluation tools obtaining models of high quality and accuracy; and 4) the structural and functional divergence between the target and the template.

Combination of homology modeling and experimental protein structure determination complement each other. Proteomics would be a good experimental approach to validate different in silico features of this study such as sequence polymorphism of different structural and functional motifs and epitopes, and its comparison in different olive cultivars, posttranslational modifications, i.e., glycosylation and phosphorylation motifs.

Olive PMEs exhibit processive catalytic activity and a differential PMEI interacting regulation

Based on the conservational analysis of the primary sequence, the 3D structures relationship, and the conservation of the catalytic mechanism among plant PMEs [21], we propose a processive catalytic mechanism for olive PMEs (Fig. 5f). The catalysis reaction is driven by two carboxylate residues in the center of catalytic cleft, D199 and D220. The reaction would occur by hydrolysis of the methyl-ester bond at the C-6 of a GalA residue present in the pectin. This may implicate a primary nucleophilic attack on the carboxymethyl carbonyl carbon of the methyl-ester of HG by the carboxylate group of a negatively charged D220 residue of the active site, stabilized by hydrogen-bonds with both side chain oxygens of R276. By analogy with other hydrolytic mechanisms, a tetrahedral negatively charged intermediate is formed, which is stabilized by an oxyanion hole created by one [42] or two [20, 21] conserved Gln side chains (Q176 and Q198). A second Asp residue (D199) acts as acid (proton donor) in the cleavage step where methanol is released. The active site is restored via extraction of a proton from an incoming water molecule by the resulting carboxylate group of the second Asp (D220), cleaving the covalent bond between the substrate and the first Asp. By its interaction with the aromatic rings, the HG chain is held in place within the substrate cleft, awaiting the next demethoxylation step. The importance of these residues for the catalytic mechanism of the PME enzymes was demonstrated through mutagenesis experiment in tobacco PME [42, 43].

The action-pattern of PME on HG remains to be elucidated, although three action patterns have been pointed out [44]. Neutral or lightly alkaline Ip PME isoforms of olive likely remove methyl esters by making blocks of demethylated pectin in a mechanism of hydrolysis of a number of successive methylated galacturonid units along the pectin

chain, creating long contiguous stretches of de-esterified GalA residues on the pectin, whereas acidic PMEs, however, demethoxylate pectin randomly [45–47]. In addition, pH or pattern of methoxylation of the pectin might also influence the mode of action [48, 49].

Control of the PME enzymatic activity is one of the major topics still under discussion. A mechanism for PME enzymatic activity control has been proposed which includes the presence of PME inhibitors (PMEIs) [50]. The high specificity of these molecules is clearly demonstrated by their inability to act toward other (poly)saccharide-degrading enzymes, such as PG, amylase and invertase [51, 52].

Docking analysis indicates that the inhibition occurs throughout the interaction of PMEI with the ligand-binding cleft of PME structure, as previously described by Di Matteo et al. for kiwi and tomato interaction model [21]. However, major differences are present between this model and the interaction model shown in the present work, particularly with regard to the residues and 3D-structural elements implicated.

This is the first time that an alternative interaction model driving the regulation of the PME catalytic activity by PMEI interaction has been described. This might indicate that differential mechanisms are possible for PME regulation, especially because of the large number of different isoforms expressed for both types of proteins, PME [7, 10] and PMEI [52, 53].

This new model of interaction is in agreement with previous observations indicating that the PMEI inhibitor was active against several plant PMEs [51, 54–58], i.e., kiwi, orange, apple, tomato, apricot, carrot, potato, banana, kaki, cucumber, strawberry and flax, whereas it did not affect bacterial and fungal PMEs [2, 39, 59, 60], possibly because of structural differences affecting the shape and the size of the cleft wall in the active site preventing the interaction.

The new model of olive PME-carrot PMEI interaction proposed in the present study has revealed significant differences in comparison with the previous model [21]. These differences include: i) residues of PMEI structure, corresponding to the α2-loop-α3 and C-terminal region are directly involved in establishment of the contact with the ligand-binding cleft; ii) key residues implicated in the catalytic reaction (D198, and D220) are involved in the contact with residues of the PMEI C-terminal region (K190) to stabilize the interaction. This new characteristic of the interaction suggests that the inhibition of the enzyme is not based only on steric impediments for joining a new pectin chain to the ligand-binding cleft, but also blocking the catalytic reaction by sequestering two residues of the PME active center implicated in the catalytic reaction. iii) Other additional areas of the PMEI structure are involved in the interaction with PME; iv) the interaction is mainly stabilized by electrostatic forces. A well-matched pattern distribution of opposite charges in both interacting surface, PME and PMEI has been described; v) no large zones of hydrophobic interactions are present.

Olive pollen PMEs contain T- and B-cell epitopes which might be relevant for their allergenic potential

Interactions among B- and T-cells play a key role in the etiology of allergic response. High quality computational tools for epitopes predictions are necessary [61, 62], and numerous databases of experimentally derived epitopes have helped in the development of algorithms for predicting epitopes of hitherto uncharacterized proteins, i.e., PDB (www.pdb.org), SDAP (fermi.utmb.edu/SDAP), Allergome (www.allergome.org). Algorithms-based epitopes prediction tools used in the present study, i.e., T-EPITOPE, have previously demonstrated high predictable accuracy, and excellent correlation with experimental data for allergens such as Bet v 1 [63], Lol p 5a from rye grass [64], Pru p 3 from peach [65], Phl p 1 from timothy grass [66], Cry j 1 from Japanese cedar [67], pathogenesis related proteins from the groups PR-10 and PR-14 [68], plant profilins [69], Art v 1 from mugwort pollen [70], and numerous other allergens.

In the present study, potential IgE and HLA class II binding regions of Ole e 11 were defined by *in silico* methods. Numerous micro-heterogeneities of the Ole e 11 isoform sequences have been located in B-cell epitopes. In addition, Ole e 11 3D models were generated not only to provide a structural localization of predicted epitopes, but also to define properties of these predicted regions. Important sequence features have been defined in the IgE binding sites, i.e., glycine and lysine have a key role in the IgE binding allergenic epitopes [71]. In addition, other studies demonstrated that allergen epitopes were comprised of a high proportion of hydrophobic amino acids [72]. The most common residues in the B-cell epitopes of Ole e 11 were lysine followed by glycine and proline. In addition, almost half of the total residues lying in B-cell epitopes were hydrophobic.

IgE binding requires partial accessibility for solvent [73]. Ole e 11 showed that more than half of residues have relative solvent accessibility of 30 % or more, indicating a possibility for immunoglobulin binding. Additional solvent accessible charged residues as arginine, glutamate or aspartate may interact with several amino acid residues facilitating subunit interaction.

Furthermore, electrostatic interactions are known to determine the orientation of the molecules and stabilize antigen-antibody complexes [74]. In the present study, the epitopes P5 and P7 showed a strong negative potential, although scattered blue regions are observed due to lysine

residues. Thus, both epitopes P5 and P7 with a strong negative potential and low hydrophobicity about 50 % are predicted to be a high affinity binder.

Epitopes P5 and P7 show nsAP**R**P**D**G**KR**VGA and **K**GPGAnM**EKR**A**K**F patterns, respectively. P5 peptide is highly conserved in allergens such as Sal k 1 (*Salsola kali*) and Der p 1 (*Dermatophagoides pteronyssinus*), and P7 peptide in allergens like Sal k 1, Cuc m 1 (*Cucumis melo*), Ara h 11 (*Arachis hypogaea*), Bet v 6 (*Betula verrucosa*), and Ses i 5 (*Sesamum indicum*) (SDAP). Thus, the patterns found in Ole e 11 peptides P5 and P7 may be relevant in determining its allergenicity.

Allergic responses are triggered through activation of CD4+ T-cells by recognizable antigenic epitopes in conjunction with HLA class II peptides. Ole e 11 isoform sequences were analyzed for identification of promiscuous HLA class II binding regions using MHC class II binding prediction methods, making them suitable for vaccine development and immunotherapy. *In silico* prediction of the binding residue(s) in the epitope and its mutagenesis to reduce allergenicity could pave the way for development of novel tools in immunoinformatics, however experimental work is required to validate these epitopes, since computational tools predicting MHC class II peptides are limited in defining T-cell identification of the bound peptides, as well as factors such as co-stimulatory molecules which are essential for induction of T-cell proliferation to the allergen molecules.

Acknowledgments This study was supported by the following European Regional Development Fund co-financed grants: MCINN BFU 2004-00601/BFI, BFU 2008-00629, BFU2011-22779, CICE (Junta de Andalucia) P2010-CVI15767, P2010-AGR6274 and P2011-CVI-7487. The funders had no role in the study, design or decision to publish.

Authors' Contributions JCJ-L conceived and designed the study. JCJ-L performed the study. JCJ-L, SOK, and JDA analyzed, discussed and assessed the resulting data. JCJ-L, SOK, and JDA contributed reagents/materials/analysis tools. JCJ-L, SOK, MIR-G, and JDA wrote the paper.

References

1. Willats WG, Orfila C, Limberg G, Buchholt HC, van Alebeek GJ, Voragen AG, Marcus SE, Christensen TM, Mikkelsen JD, Murray BS, Knox JP (2001) Modulation of the degree and pattern of methyl-esterification of pectic homogalacturonan in plant cell walls. Implications for pectin methyl esterase action, matrix properties, and cell adhesion. J Biol Chem 276:19404–19413
2. Giovane A, Servillo L, Balestrieri C, Raiola A, D'Avino R, Tamburrini M, Clardiello MA, Camardella L (2004) Pectin methylesterase inhibitor. Biochim Biophys Acta 1696:245–252
3. Rexova-Benkova L, Markovic O (1976) Pectic enzymes. Adv Carbohydr Chem Biochem 33:323–385
4. Benen JAE, Vincken JP, van Alebeek GJ (2002) Microbial pectinases. In: Seymour GB, Knox JP (eds) Pectins and their manipulation. Blackwell, Oxford, pp 174–221
5. Shen ZC, Pappan K, Mutti NS, He QJ, Denton M, Zhang Y, Kanost MR, Reese JC, Reeck GR (2005) Pectinmethylesterase from the rice weevil, Sitophilus oryzae: cDNA isolation and sequencing, genetic origin, and expression of the recombinant enzyme. J Insect Sci 5:21
6. Benen JAE, van Alebeek GJWM, Voragen AGJ, Visser J (2003) Pectic esterases. In: Whitaker JR, Voragen AGJ, Wong DWS (eds) Handbook of food enzymology. Dekker, New York, pp 849–856
7. Micheli F, Sundberg B, Goldberg R, Richard L (2000) Radial distribution pattern of pectin methylesterases across the cambial region of hybrid aspen at activity and dormancy. Plant Physiol 124:191–199
8. Pilling J, Willmitzer L, Bücking H, Fisahn J (2004) Inhibition of a ubiquitously expressed pectin methyl esterase in Solanum tuberosum L. affects plant growth, leaf growth polarity, and ion partitioning. Planta 219(1):32–40
9. Siedlecka A, Wiklund S, Péronne MA, Micheli F, Lesniewska J, Sethson I, Edlund U, Richard L, Sundberg B, Mellerowicz EJ (2008) Pectin methyl esterase inhibits intrusive and symplastic cell growth in developing wood cells of Populus. Plant Physiol 146:554–565
10. Micheli F (2001) Pectin methylesterases: cell wall enzymes with important roles in plant physiology. Trends Plant Sci 6(9):414–419
11. Krichevsky A, Kozlovsky SV, Tian GW, Chen MH, Zaltsman A, Citovsky V (2007) How pollen tubes grow. Dev Biol 303:405–420
12. Collmer A, Keen NT (1986) The role of pectic enzymes in plant pathogenesis. Annu Rev Phytopathol 24:383–409
13. Dorokhov YL, Frolova OY, Skurat EV, Ivanov PA, Gasanova TV, Sheveleva AA, Ravin NV, Makinen KM, Klimyuk VI, Skryabin KG, Gleba YY, Atabekov JG (2006) A novel function for a ubiquitous plant enzyme pectin methylesterase: the enhancer of RNA silencing. FEBS Lett 580:3872–3878
14. Will-Karp M, Santeliz J, Karp CL (2001) The germless theory of allergic disease: revisiting the hygiene hypothesis. Nat Rev Immunol 1(1):69–75
15. Esteve C, Montealegre C, Marina ML, García MC (2012) Analysis of olive allergens. Talanta 92:1–14
16. Salamanca G, Rodríguez R, Quiralte J, Moreno C, Pascual CY, Barber D, Villalba M (2010) Pectin methylesterases of pollen tissue, a major allergen in olive tree. FEBS J 277(13):2729–2739
17. Wu S, Zhang Y (2010) SEGMER: identifying protein substructural similarity by segmental threading. Structure 18:858–867
18. Kozakov D, Hall DR, Beglov D, Brenke R, Comeau SR, Shen Y, Li K, Zheng J, Vakili P, Paschalidis IC, Vajda S (2010) Achieving reliability and high accuracy in automated protein docking: Cluspro, PIPER, SDU, and stability analysis in CAPRI rounds 13–19. Proteins 78:3124–3130
19. Markovic O, Janecek S (2004) Pectin methylesterases: sequence-structural features and phylogenetic relationships. Carbohydr Res 339:2281–2295
20. Johansson K, El-Ahmad M, Friemann R, Jörnvall H, Markovic O, Eklund H (2002) Crystal structure of plant pectin methylesterase. FEBS Lett 514(2–3):243–249
21. Di Matteo A, Giovane A, Raiola L, Camardella D, Bonivento G, De Lorenzo F, Cervone D, Bellincampi D, Tsernoglou (2005) Structural basis for the interaction between pectin methylesterase and a specific inhibitor protein. Plant Cell 17:849–858
22. Sarika AM, Akram M, Iquebal MA, Naimuddin K (2010) Prediction of MHC binding peptides and epitopes from coat protein of mungbean yellow mosaic india virus-Ub05. J Proteomics Bioinform 3:173–178
23. Gomase VS, Waghmare SB, Jadhav B, Kale KV (2009) Mapping of MHC class binding nonamers from lipid binding protein of Ascaridia galli. Gene Ther Mol Biol 13:10–14
24. Thonar C, Liners F, Van Cutsem P (2006) Polymorphism and modulation of cell wall esterase enzyme activities in the chicory root during the growing season. J Exp Bot 57(1):81–89

25. Bordenave M (1996) Analysis of pectin methyl esterases. In: Linskens HF, Jackson JF (ed) Plant cell wall analysis (Modern methods of plant analysis). Springer, Heidelberg, pp 165–180
26. Ding JLC, Hsu JSF, Wang MMC, Tzen JTC (2002) Purification and glycosylation analysis of an acidic pectin methylesterase in jelly fig (*Ficus awkeotsang*) achenes. J Agric Food Chem 50 (10):2920–2925
27. Bosch M, Hepler PK (2005) Pectin methylesterases and pectin dynamics in pollen tubes. Plant Cell 17(12):3219–3226
28. Bosch M, Cheung AY, Hepler PK (2005) Pectin methylesterase, a regulator of pollen tube growth. Plant Physiol 138(3):1334–1346
29. Pelloux J, Rusterucci C, Mellerowicz EJ (2007) New insights into pectin methylesterase structure and function. Trends Plant Sci 12 (6):267–277
30. Hamman-Khalifa A, Castro AJ, Jimenez-Lopez JC, Rodríguez-García MI, Alché JD (2008) Olive cultivar origin is a major cause of polymorphism for Ole e 1 pollen allergen. BMC Plant Biol 8:10
31. Jimenez-Lopez JC, Morales S, Castro AJ, Volkmann D, Rodríguez-García MI, Alché JD (2012) Characterization of profilin polymorphism in pollen with a focus on multifunctionality. PLoS One 7(2):e30878
32. Dorokhov YL, Skurat EV, Frolova OY, Gasanova TV, Ivanov PA, Ravin NV, Skryabin KG, Makinen KM, Klimyuk VI, Gleba YY, Atabekov JG (2006) Role of the leader sequence in tobacco pectin methylesterase secretion. FEBS Lett 580(13):3329–3334
33. Ciardiello MA, D'Avino R, Amoresano A, Tuppo L, Carpentieri A, Carratore V, Tamburrini M, Giovane A, Pucci P, Camardella L (2008) The peculiar structural features of kiwi fruit pectin methylesterase: amino acid sequence, oligosaccharides structure, and modeling of the interaction with its natural proteinaceous inhibitor. Proteins 71(1):195–206
34. Giovane A, Quagliuolo L, Castaldo D, Servillo L, Balestrieri C (1990) Pectin methyl esterase from Actinidia chinensis fruits. Phytochemistry 29:2821–2823
35. Randall GD, Karel GJ (1996) Purification and characterization of a thermally tolerant pectin methylesterase from a commerical Valencia fresh frozen orange juice. Agric Food Chem 44:458–462
36. Hsiao ES, Chen JC, Tsai HY, Khoo KH, Chen ST, Tzen JT (2009) Determination of N-glycosylation site and glycan structures of pectin methylesterase in jelly fig (*Ficus awkeotsang*) Achenes. J Agric Food Chem 57(15):6757–6763
37. Warren ME, Kester H, Benen J, Colangelo J, Visser J, Bergmann C, Orlando R (2002) Studies on the glycosylation of wild-type and mutant forms of Aspergillus niger pectin methylesterase. Carbohydr Res 337(9):803–812
38. Markovic O, Jornvall H (1992) Disulfide bridges in tomato pectinesterase - variations from pectinesterases of other species - conservation of possible active-site segments. Protein Sci 1 (10):1288–1292
39. D'Avino R, Camardella L, Christensen TMIE, Giovane A, Servillo L (2003) Tomato pectin methylesterase: modeling, fluorescence, and inhibitor interaction studies - comparison with the bacterial (*Erwinia chrysanthemi*) enzyme. Proteins 53(4):830–839
40. Jenkins J, Mayans O, Smith D, Worboys K, Pickersgill RW (2001) Three-dimensional structure of Erwinia chrysanthemi pectin methylesterase reveals a novel esterase active site. J Mol Biol 305 (4):951–960
41. Johansson K, El-Ahmad M, Friemanna R, Jornvall H, Markovic O, Eklund H (2002) Crystal structure of plant pectin methylesterase. FEBS Lett 514(2–3):243–249
42. Fries M, Ihrig J, Brocklehurst K, Shevchik VE, Pickersgill RW (2007) Molecular basis of the activity of the phytopathogen pectin methylesterase. EMBO J 26:3879–3887
43. Duwe B, Khanh NQ (1996) Site-directed mutagenesis of the active site of pectin methylesterase from Aspergillus niger RH5344. Biotechnol Lett 18(6):621–626
44. Greenwood CT, Milne EA (1968) Starch degrading and synthesizing enzymes: a discussion of their properties and action patterns. Adv Carbohydr Chem Biochem 23:282–366
45. Limberg G, Korner R, Buchholt HC, Christensen TMIE, Roepstorff P, Mikkelsen JD (2000) Analysis of pectin structure part 1 - analysis of different deesterification mechanisms for pectin by enzymatic fingerprinting using endopectin lyase and endopolygalacturonase II from A. niger. Carbohydr Res 327(3):293–307
46. Ralet MC, Dronnet V, Buchholt HC, Thibault JF (2001) Enzymatically and chemically de-esterified lime pectins: characterisation, polyelectrolyte behaviour and calcium binding properties. Carbohydr Res 336(2):117–125
47. Duvetter T, Fraeye I, Sila DN, Verlent I, Smout C, Hendrickx M, Van Loey A (2006) Mode of de-esterification of alkaline and acidic pectin methyl esterases at different pH conditions. J Agric Food Chem 54(20):7825–7831
48. Goldberg R, Pierron M, Bordenave M, Breton C, Morvan C, du Penhoat CH (2001) Control of mung bean pectinmethylesterase isoform activities - influence of pH and carboxyl group distribution along the pectic chains. J Biol Chem 276(12):8841–8847
49. Kim Y, Teng Q, Wicker L (2005) Action pattern of Valencia orange PME deesterification of high methoxyl pectin and characterization of modified pectins. Carbohydr Res 340(17):2620–2629
50. Irifune K, Nishida T, Egawa H, Nagatani A (2004) Pectin methylesterase inhibitor cDNA from kiwi fruit. Plant Cell Rep 23(5):333–338
51. Balestrieri C, Castaldo D, Giovane A, Quagliuolo L, Servillo L (1990) A glycoprotein inhibitor of pectin methylesterase in kiwi fruit (Actinidia chinensis). Eur J Biochem 193:183–187
52. Camardella L, Carratore V, Ciardiello MA, Servillo L, Balestrieri C, Giovane A (2000) Kiwi protein inhibitor of pectin methylesterase. Amino-acid sequence and structural importance of two disulfide bridges. Eur J Biochem 267(14):4561–4565
53. Mattei B, Raiola A, Caprari C, Federici L, Bellincampi D, De Lorenzo G, Cervone F, Giovane A, Camardella L (2002) Studies on plant inhibitors of pectin modifying enzymes: Polygalacturonase-inhibiting protein (PGIP) and pectin methylesterase inhibitor (PMEI). In: Teeri TT, Svensson B, Gilbert HJ, Feizi T (eds) Carbohydrate bioengineering: interdisciplinary approaches. Royal Society of Chemistry, Cambridge, pp 160–167
54. Giovane A, Balestrieri C, Quagliuolo L, Castaldo D, Servillo L (1995) A glycoprotein inhibitor of pectin methylesterase in kiwi fruit - purification by affinity chromatography and evidence of a ripening-related precursor. Eur J Biochem 233(3):926–929
55. Jiang CM, Lai YJ, Chang WH, Wu MC, Chang HM (2001) Pectinesterase inhibitor in jelly fig (*Ficus awkeotsang Makino*) achenes. J Food Sci 66:225–228
56. Jiang CM, Li CP, Chang JC, Chang HM (2002) Characterization of pectinesterase inhibitor in jelly fig (Ficus awkeotsang Makino) achenes. J Agric Food Chem 50:4890–4894
57. Ciardiello MA, Tamburrini M, Tuppo L, Carratore V, Giovane A, Mattei B, Camardella L (2004) Pectin methylesterase from kiwi and kaki fruits: purification, characterization, and role of pH in the enzyme regulation and interaction with the kiwi proteinaceous inhibitor. J Agric Food Chem 52(25):7700–7703
58. Dedeurwaerder S, Menu-Bouaouiche L, Mareck A, Lerouge P, Guerineau F (2009) Activity of an atypical Arabidopsis thaliana pectin methylesterase. Planta 229(2):311–321
59. McMillan GP, Perombelon MCM (1995) Purification and characterization of a high pI pectin methylesterase isozyme and its inhibitor from tubers of Solanum tuberosum subsp. Tuberosum cv. Katahdin. Physiol Mol Plant Pathol 46:413–427
60. Duvetter T, Van Loey A, Smout C, Verlent I, Ly-Nguyen B, Hendrickx M (2005) Aspergillus aculeatus pectin methylesterase: study of the inactivation by temperature and pressure and the inhibition by pectin methylesterase inhibitor. Enzyme Microb Technol 36(4):385–390

61. Wang P, Sidney J, Dow C, Mothe B, Sette A, Peters B (2008) A systematic assessment of MHC class II peptide binding predictions and evaluation of a consensus approach. PLoS Comput Biol 4: e1000048
62. Blythe MJ, Flower DR (2005) Benchmarking B cell epitope prediction: underperformance of existing methods. Protein Sci 14:246–248
63. Dall'Antonia F, Gieras A, Devanaboyina SC, Valenta R, Keller W (2011) Prediction of IgE-binding epitopes by means of allergen surface comparison and correlation to cross-reactivity. Prediction of IgE-binding epitopes by means of allergen surface comparison and correlation to cross-reactivity. J Allergy Clin Immunol 128(4):872–879
64. de Lalla C, Sturniolo T, Abbruzzese L, Hammer J, Sidoli A, Sinigaglia F, Panina-Bordignon P (1999) Cutting edge: identification of novel T cell epitopes in Lol p5a by computational prediction. J Immunol 163:1725–1729
65. García-Casado G, Pacios LF, Díaz-Perales A, Sánchez-Monge R, Lombardero M, García-Selles FJ, Polo F, Barber D, Salcedo G (2003) Identification of IgE-binding epitopes of the major peach allergen Pru p 3. J Allergy Clin Immunol 112(3):599–605
66. Ball T, Fuchs T, Sperr WR, Valent P, Vangelista L, Kraft D, Valenta R (1999) B-cell epitopes of the major timothy grass pollen allergen, Phl p 1, revealed by gene fragmentation as candidates for immunotherapy. FASEB J 13:1277–1290
67. Midoro-Horiuti T, Schein CH, Mathura V, Braun W, Czerwinski EW, Togawa A, Kondo Y, Oka T, Watanabe M, Goldbluma RM (2006) Structural basis for epitope sharing between group 1 allergens of cedar pollen. Mol Immunol 43(6):509–518
68. Jimenez-Lopez JC, Gachomo WE, Ariyo O, Baba-Moussa L, Kotchoni SO (2012) Specific conformational epitope features of pathogenesis-related proteins mediating cross-reactivity between pollen and food allergens. Mol Biol Rep 39(1):123–130
69. Radauer C, Willerroiderw M, Fuchs H, Hoffmann K, Thalhamerw J, Ferreira F, Scheiner O, Breiteneder H (2006) Cross-reactive and species-specific immunoglobulin E epitopes of plant profilins: an experimental and structure-based analysis. Clin Exp Allergy 36:920–929
70. Jahn-Schmid B, Kelemen P, Himly M, Bohle B, Fischer G, Ferreira F, Ebner C (2002) The T cell response to art v 1, the major mugwort pollen allergen, is dominated by one epitope. J Immunol 169:6005–6011
71. Oezguen N, Zhou B, Negi SS, Ivanciuc O, Schein CH, Labesse G, Braun W (2008) Comprehensive 3D-modeling of allergenic proteins and amino acid composition of potential conformational IgE epitopes. Mol Immunol 45:3740–3747
72. Wolff N, Yannai S, Karin N, Levy Y, Reifen R, Dalal I, Cogan U (2004) Identification and characterization of linear B-cell epitopes of beta-globulin, a major allergen of sesame seeds. J Allergy Clin Immunol 114:1151–1158
73. Brinda KV, Vishveshwara S (2005) Oligomeric protein structure networks: insights into protein-protein interactions. BMC Bioinforma 6:296
74. Sinha N, Mohan S, Lipschultz CA, Smith-Gill SJ (2002) Differences in electrostatic properties at antibody-antigen binding sites: implications for specificity and cross-reactivity. Biophys J 83:2946–2968